Geological Quarterly, 2023, 67: 49
DOI: http://dx.doi.org/10.7306/gq.1719

Colours of the upper Neogene "Poznań Clays" in the light of sedimentological, mineralogical and nuclear methods

Jakub KLĘSK[1, *], Artur BŁACHOWSKI[2], Łukasz KRUSZEWSKI[3], Danuta MICHALSKA[1], Małgorzata MROZEK-WYSOCKA[1] and Marek WIDERA[1]

[1] Adam Mickiewicz University, Institute of Geology, Krygowskiego 12, 61-680 Poznań, Poland, ORCID: 0000-0001-7437-1232 [J.K.], 0000-0002-9893-4527 [D.M.], 0000-0002-8194-4331 [M.M.-W.], 0000-0001-5092-2845 [M.W.]

[2] AGH University, Faculty of Geology, Geophysics and Environmental Protection, al. Mickiewicza 30, 30-059 Kraków, Poland, ORCID: 0000-0002-5591-5756 [A.B.]

[3] Polish Academy of Sciences, Institute of Geological Sciences, Twarda 51/55, 00-818 Warszawa, Poland, ORCID: 0000-0001-6332-9944 [Ł.K.]

Klęsk, J., Błachowski, A., Kruszewski, Ł., Michalska, D., Mrozek-Wysocka, M., Widera, M., 2023. Colours of the upper Neogene "Poznań Clays" in the light of sedimentological, mineralogical and nuclear methods. Geological Quarterly, 67: 49; https://doi.org/10.7306/gq.1719

The Miocene–Pliocene overbank facies "Poznań Clays" are particularly well exposed in large lignite outcrops in central Poland, for example, in the Jóźwin IIB opencast mine. During their accumulation the climate fluctuated from moderately warm and humid to cool and dry. In general, the dark grey and the greyish-violet colours come from macroscopically visible organic matter and the absence of hematite and/or goethite. The organic matter also affects the Fe^{3+}/Fe^{2+} ratio and, consequently, the redox conditions. When the study area was poorly drained, there were favourable conditions for plant vegetation, resulting in Histosols (hydromorphic palaeosols). In a reducing environment, other sediments with "cold" colours (greenish to bluish shades) formed that included pyrite and/or gypsum, though with few or no pigments such as hematite, goethite or jarosite. At that time, elemental sulphur could also crystallize, occasionally giving a yellowish shade to the sediment mottles. When the area was well drained, most of the organic matter decayed, and the Fe^{3+}/Fe^{2+} ratio was relatively high due to progressive weathering. Under such conditions, Vertisols developed with "warm" colours (from yellow to cherry-red), enriched in hematite and goethite, and also containing gypsum and native sulphur.

Key words: varicoloured sediments, organic matter, mineral composition, iron compounds, redox conditions, climate fluctuations.

INTRODUCTION

The colour of sediment or rock is the most obvious lithological feature to the human eye (Mancini et al., 2020). Therefore, it was noted in ancient cultures that used multicoloured fine-grained sediments (e.g., clays or loams) for various practical applications. These included pigments for colour paints, artistic works, ceramics and glass, and also medical treatments and the production of building ceramics (e.g., Hartemink, 2009; Valanciene et al., 2010; Habashi, 2016). The scenic beauty of varicoloured rocks and sediments, including palaeosols, is important, too, for the tourism industry and geoheritage research (Retallack and Broz, 2020; Ruban et al., 2021). Furthermore, colour has been widely recognised as a sensitive indicator of the palaeoenvironmental conditions that prevailed during sediment accumulation, soil formation and diagenesis since the 1920s (cf. McBride, 1974; Torrent et al., 1980; Turner, 1980; Myrow, 1990; Cornell and Schwertmann, 2003; Tucker, 2011).

In the case of terrestrial sediments of different colours, research initially focused mainly on modern soils. As summarised by Bown and Kraus (1987) and Kraus (1999), pre-Quaternary palaeosol horizons are known, although a long-held prevailing view was that their preservation potential is low and that they are rarely found in the rock record. In the field, the best evidence for the occurrence of palaeosols comes from multi-coloured, horizontally arranged bands, mainly resulting from factors including the redistribution of iron compounds. Currently, there are many palaeosols that developed on bedrock of various types (fluvial, aeolian, deltaic, volcanic) in various climatic zones and of various ages, from the Precambrian to the Quaternary (e.g., Nemec and Porębski, 1977; Bown and Kraus, 1981; Schwertmann, 1985, 1993; Kraus and Aslan, 1993; PiPujol and Buurman, 1994; Kraus, 1999; Kraus and Riggins, 2007; Srivastava et al., 2013; Spinola et al., 2018; Retallack, 2019; Upreti and Srivastava, 2019; Retallack and Broz, 2020).

* Corresponding author: e-mail: jakub.klesk@amu.edu.pl

Received: May 30, 2023; accepted: October 19, 2023; first published online: December 27, 2023

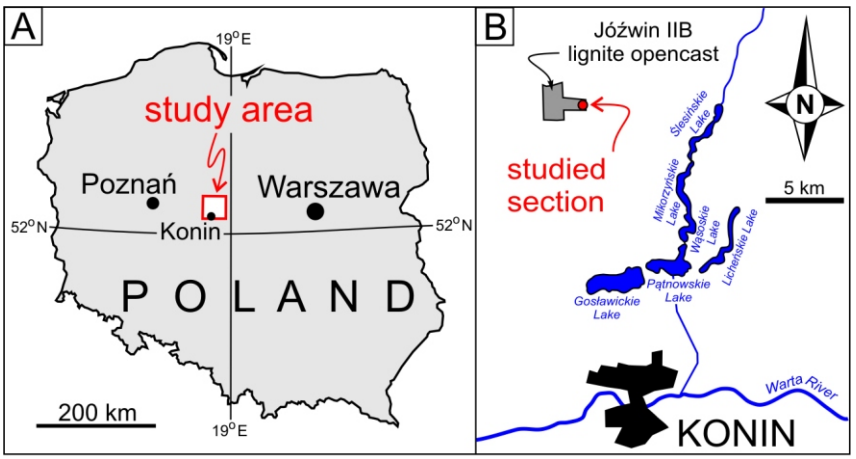

Fig. 1. Location sketch

A – study area within Poland; **B** – location of the Jóźwin IIB lignite opencast mine (Konin Lignite Mine, central Poland) with the section studied

Many studies have been devoted, too, to the colours of marine sediments, as summarised by, for example, Bábek et al. (2021, 2022), Jiang et al. (2022) and Card and Montenari (2023).

Opencast lignite mining in central Poland has long made possible direct observations of the varicoloured "Poznań Clays" that include distinct palaeosol horizons (see the Appendix). The research conducted so far has focused on the mineralogy of these deposits, and in particular on the mineral composition of their clay fraction (e.g., Wiewióra and Wyrwicki, 1974, 1976; Wyrwicki, 1975; Górniak et al., 2001; Duczmal-Czernikiewicz, 2010, 2013; Ratajczak et al., 2015). Over the last decade, however, sedimentological studies concerned with palaeoclimatic and palaeotectonic issues of the "Poznań Clays" have dominated (e.g., Maciaszek et al., 2019, 2020; Widera et al., 2019, 2021a, b; Zieliński and Widera, 2020; Kędzior et al., 2021). Nevertheless, apart from our preliminary studies (Klęsk et al., 2022; Klęsk, 2023), none of the contributions to date have focused on interpreting the colour patterns of these deposits.

In this paper we: (1) give a brief sedimentological description of the multi-coloured fine-grained deposits; (2) determine the mineral composition, as well as the valence state of iron, in beds of different colour; and (3) interpret the origin of various colours of the "Poznań Clays" in the context of their fluvial origin and of late Neogene climate changes.

MATERIALS AND METHODS

LITHOLOGICAL DESCRIPTION AND GEOLOGICAL BACKGROUND

Until the 1960s, the "Poznań Clays" were thought to have formed in a "Pliocene Lake" (e.g., Areń, 1964). Then, a few thin layers of marine and fluvial facies were documented within these fine-grained lacustrine deposits (Dyjor, 1970; Ciuk and Pożaryska, 1982). Thus, a lacustrine-fluvial-marine hypothesis dominated for the next 3–4 decades. At the beginning of the 21st century, a fluvial origin for the "Poznań Clays" was proposed, mainly on the basis of borehole data (Badura and Przybylski, 2004; Piwocki et al., 2004).

The varicoloured deposits studied in this paper accumulated in the overbank zone of a late Neogene river system. This interpretation is supported by numerous (>30) river palaeochannels (sandy, sandy-muddy to muddy) within the "Poznań Clays" that were documented in lignite opencast mines, including the Jóźwin IIB opencast mine, in central Poland (Widera et al., 2017, 2021b; Zieliński and Widera, 2020; Kędzior et al., 2021). The presence of interbeds enriched in organic matter, and even lignite beds (see the Appendix) or seams (the accompanying 1a Oczkowice and 0 Orłowo lignite seams), also demonstrates their terrestrial origin (Widera, 2007, 2021; Maciaszek et al., 2020). In addition, slickenside structures (typical for Vertisols), documented by Duczmal-Czernikiewicz (2013), indicate periodic drainage and wetting of fine-grained sediments in dry and humid subaerial conditions, respectively. This influenced the mineral composition and particularly the clay fraction. The average smectite and "illite"-smectite content among the clay fraction of the "Poznań Clays" is up to 60% (Górniak et al., 2001), and it may even be as high as 80% in individual samples (Duczmal-Czernikiewicz, 2010, 2013). These minerals were previously classified as beidellite (Wiewióra and Wyrwicki, 1976), which forms in terrestrial environments as a result of weathering in palaeosol conditions (e.g., Wiewióra and Wyrwicki, 1974; Wyrwicki, 1975; Środoń et al., 2014; Retallack, 2019).

The section examined during fieldwork in June 2021 was situated in the eastern part of the Jóźwin IIB lignite opencast mine. Its geographic co-ordinates are as follows: 52°24'25.7''N and 18°11'53.6''E. The study area is part of the Konin Lignite Mine, which operates near the town of Konin in central Poland (Fig. 1). Due to lignite mining, the Neogene sub- and supra-lignite strata, including the Quaternary, were exposed. Lithostratigraphically, the Neogene includes only two main units, the Koźmin and Poznań formations (Widera, 2007). The Koźmin Formation comprises mainly fluvial sands that underlie the 1st Mid-Polish Lignite Seam (MPLS-1), exploited for electricity production. The Poznań Formation is divided into the lower Grey Clays Member and the upper Wielkopolska Member (e.g., Piwocki and Ziembińska-Tworzydło, 1997; Widera, 2007, 2021).

The Grey Clays Member contains mainly the MPLS-1 lignite seam (>99 vol.%), which is 3–13 m thick, its average thickness in the study area being 6.6 m (Maciaszek et al., 2019; Widera, 2021), and discontinuous lenses of "grey clays" (<1 vol.%), with dispersed organic matter and xylites (i.e., fossilised wood fragments >1 cm in size) locally in its roof. By contrast, the Wielkopolska Member is predominantly (>95 vol.%) made up of

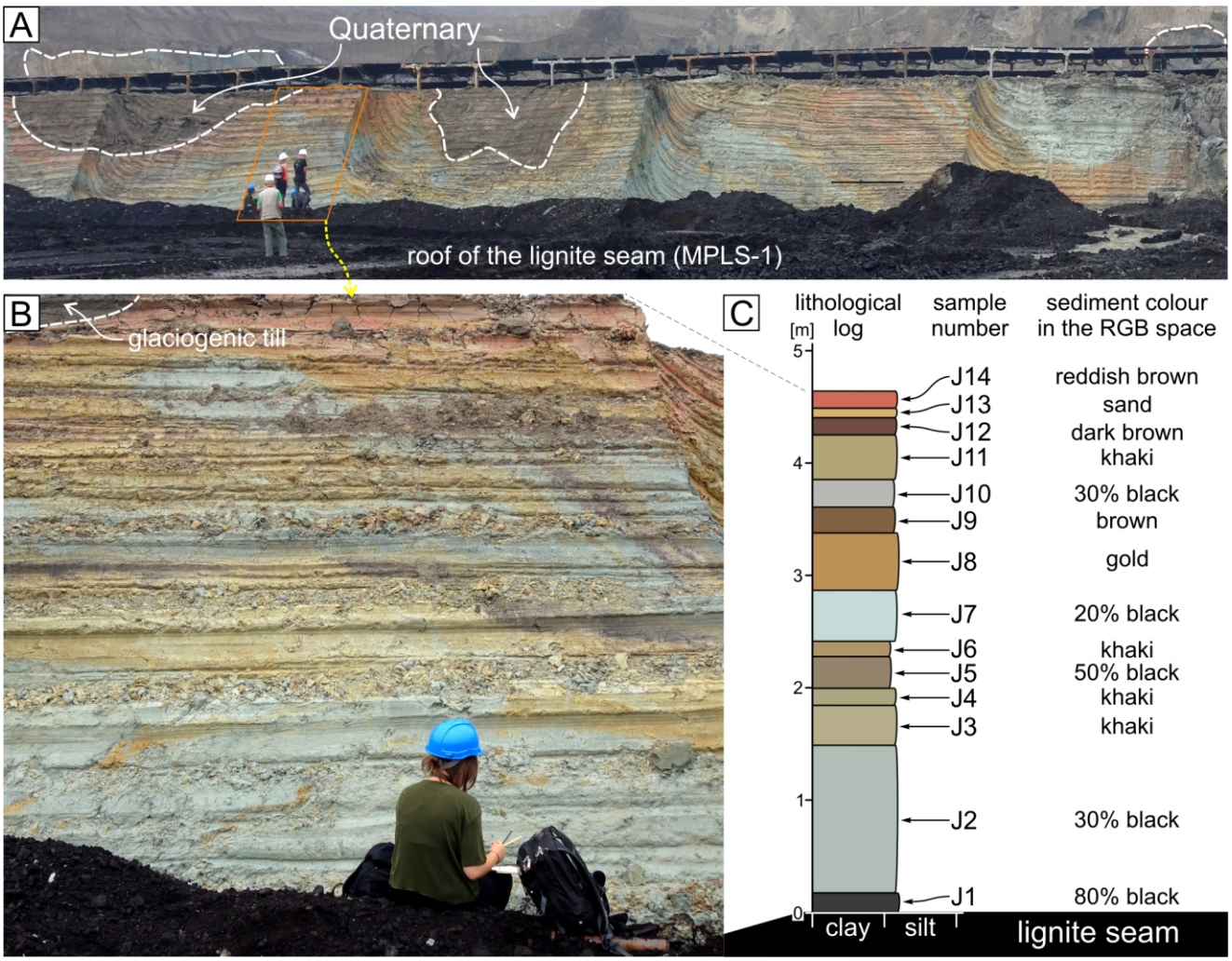

Fig. 2. Varicoloured "Poznań Clays" in the Jóźwin IIB opencast mine (June 2021)

A – broad eastwards view of the exposure, note glaciotectonically folded "Poznań Clays" and Quaternary deposits; **B** – close-up view of the section studied; **C** – the corresponding lithological log with sampling points and sediment colour in the RGB space; the RGB colour name is created automatically by the CorelDRAW X8 software; for more data, see Table 1

varicoloured overbank muds ("green clays" and "flame-like clays"), as well as channel-fill (<5 vol.%) sands and muds (Widera et al., 2019; Maciaszek et al., 2020; Zieliński and Widera, 2020; Kędzior et al., 2021). Due to Pleistocene glaciotectonics and erosion, the Wielkopolska Member ranges from a few to >30 m thick in the Jóźwin IIB lignite opencast mine (Widera et al., 2017); the section examined in detail is ~4.7 m thick (Fig. 2).

In brief, the "Poznań Clays" examined include both "grey clays" (uppermost Grey Clays Member) and "green clays" and "flame-like clays" (Wielkopolska Member; Ciuk, 1970; Dyjor, 1970; Piwocki and Ziembińska-Tworzydło, 1997). These accumulated from the latest Mid-Miocene to the earliest Pliocene, that is, from ~14.3 to 5 Ma (Kędzior et al., 2021; Widera et al., 2021a, b). Moving from the base to the top of the exposed wall, 14 samples were taken for laboratory analyses from each stratum that possessed a distinct colour (Fig. 2). The colour of the samples was initially and subjectively described in the field. The sampling took place after it had rained; hence, the colour of the sediment in the samples (fresh and moist) and the colour of the sediment in the exposed wall (wet) differed significantly.

LABORATORY RESEARCH METHODS

COLOUR DESCRIPTION

Munsell's Rock Colour Book (2012) and CorelDRAW X8 software were applied to objectively determine the colour of the sediment. The air-dried and powdered samples were first photographed, and then their colour was evaluated using the

Fig. 3. Powdered samples J1–J14 used for further analyses and to evaluate their homogenised colours of different hues

For details, see Table 1

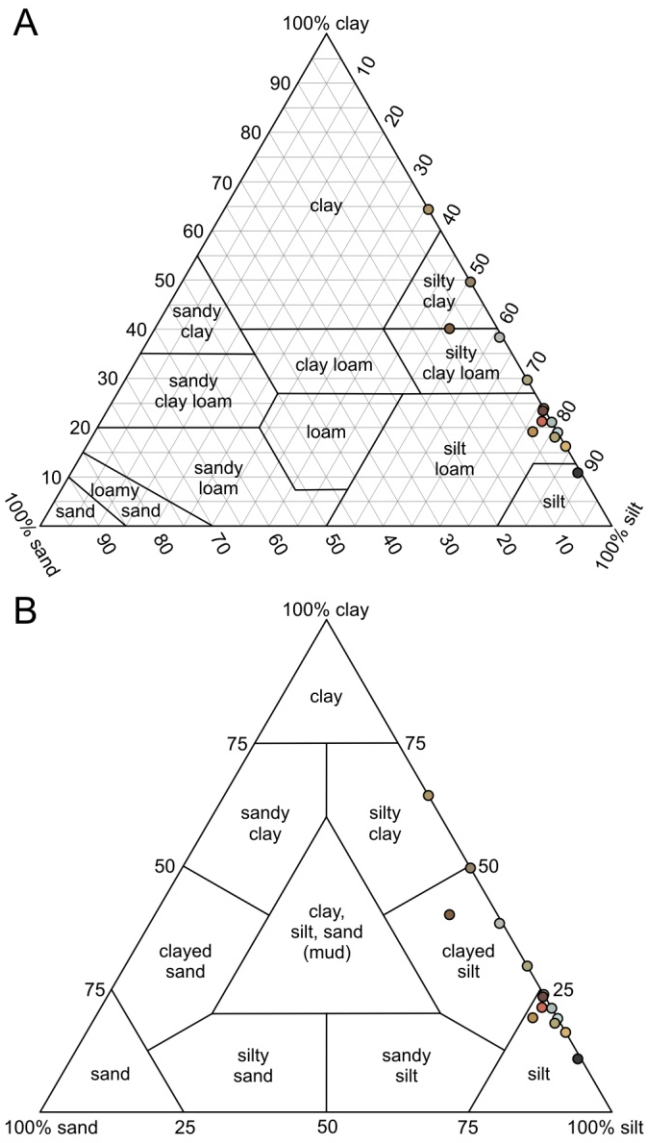

Fig. 4. Nomenclature of the sediment in different classification triangles

A – soil textural classes in the USDA classification system (Retallack, 2019); **B** – textural classes of fine-grained sediments in the classification of Shepard (1954); note the different nomenclature and various values for critical boundaries; for details, see Table 2

Munsell and RGB (red-green-blue) systems (Fig. 3 and Table 1). It is becoming more and more common for the colours of soils, sediments and rocks to be determined automatically in a digitised form, both in the RGB system and in other colour spaces such as CMYK and CIELAB (e.g., Mancini et al., 2020; Klęsk et al., 2022).

GRAIN SIZE AND ORGANIC CONTENT ANALYSIS

A particle-size analysis was performed using laser diffraction at the Department of Geomorphology at Adam Mickiewicz University in Poznań, Poland. A Malvern Mastersizer 2000 analyzer was used, and each result was expressed as a percentage by volume. As a result, the clay (<2 μm), silt (2–63 μm) and sand (>63 μm) fractions in the bulk samples were determined. The mean grain size of the sediment was determined using *GRADISTAT 5.11* software.

The sediment name for each sample was defined according to the United States Department of Agriculture (USDA) classification system (cf. Retallack, 2019, his fig. 3.10), which is mainly used by soil researchers, and according to the Shepard (1954) classification scheme, which is preferred by sedimentologists and more generally by geologists (Fig. 4 and Table 2). The presence of organic matter in samples J1 and J10 was confirmed by applying hot 30% hydrogen peroxide (H_2O_2) for several minutes.

Table 1

Comparison of the sediment colours determined in the field, in the Munsell and digitised RGB (red–green–blue) systems

Sample number	Colour in the field	Air-dried sample		Dry and powdered sample	
		Munsell colour	RGB colour	Munsell colour	RGB colour
J1	dark grey (+organics)	black (N1)	80% black (R:60 G:58 B:56)	greyish black (N2)	70% black (R:67 G:63 B:63)
J2	greyish blue	medium bluish grey (5B 5/1)	30% black (R:177 G:190 B:183)	medium grey (N5)	30% black (R:158 G:168 B:182)
J3	yellow	dusty yellow (5Y 6/4)	khaki (R:182 G:174 B:139)	very pale orange (10YR 8/2)	10% black (R:222 G:222 B:203)
J4	green	light olive grey (5Y 5/2)	khaki (R:171 G:166 B:128)	light olive grey (5Y 5/2)	40% black (R:180 G:185 B:169)
J5	brown	dark yellowish brown (10YR 4/2)	50% black (R:149 G:132 B:108)	brownish grey (5YR 4/1)	50% black (R:122 G:119 B:120)
J6	yellow	moderate yellow (5Y 7/6)	khaki (R:174 G:149 B:106)	greyish orange (10YR 7/4)	khaki (R:173 G:172 B:130)
J7	bluish grey	greenish grey (5GY 6/1)	20% black (R:197 G:128 B:217)	medium light grey (N6)	20% black (R:193 G:208 B:214)
J8	yellow	dark yellowish orange (10YR 6/6)	gold (R:188 G:145 B:87)	dark yellowish orange (10YR 6/6)	khaki (R:152 G:130 B:82)
J9	brown	moderate brown (5YR 4/4)	brown (R:130 G:97 B:69)	moderate reddish brown (10R 4/6)	30% black (R:186 G:164 B:145)
J10	greyish violet	light grey (N7)	30% black (R:184 G:185 B:197)	dark grey (N3)	50% black (R:136 G:137 B:140)
J11	yellow	dusty yellow (5Y 6/4)	khaki (R:178 G:165 B:119)	greyish brown (5Y 8/4)	30% black (R:189 G:185 B:161)
J12	cherry	dusty red (5R 4/6)	dark brown (R:112 G:76 B:67)	pale yellowish orange (10YR 8/6)	sand (R:210 G:189 B:145)
J13	orange	greyish orange (10YR 7/4)	sand (R:214 G:178 B:115)	yellowish grey (5Y 7/2)	khaki (R:178 G:175 B:143)
J14	red	pale reddish brown (10R 5/4)	reddish brown (R:206 G:108 B:89)	moderate red (5R 4/6)	brown (R:154 G:122 B:102)

Table 2

Grain-size distribution and nomenclature of the sediment

Sample number	Sediment grain size [vol.%]			Mean grain size [μm]	Soil name*	Sediment name**
	clay <2 μm	silt 2–63 μm	sand >63 μm			
J1	11.37	87.99	0.64	9.1	silt	silt
J2	20.93	79.07	0.00	8.1	silt loam	silt
J3	23.88	76.12	0.00	7.9	silt loam	silt
J4	29.77	70.23	0.00	7.5	silty clay loam	clayed silt
J5	49.49	50.51	0.00	5.2	silty clay	clayed silt
J6	64.21	35.79	0.00	4.7	clay	silty clay
J7	18.84	81.16	0.00	8.1	silt loam	silt
J8	18.99	76.16	4.86	8.8	silt loam	silt
J9	40.00	51.68	8.33	7.6	silty clay	clayed silt
J10	38.03	61.50	0.47	6.7	silty clay loam	clayed silt
J11	17.89	80.99	1.12	8.3	silt loam	silt
J12	23.10	76.83	0.07	8.0	silt loam	silt
J13	16.62	83.34	0.03	8.1	silt loam	silt
J14	20.95	77.29	1.75	8.3	silt loam	silt

* – according to the USDA classification system (Retallack, 2019); ** – according to the classification scheme of Shepard (1954)

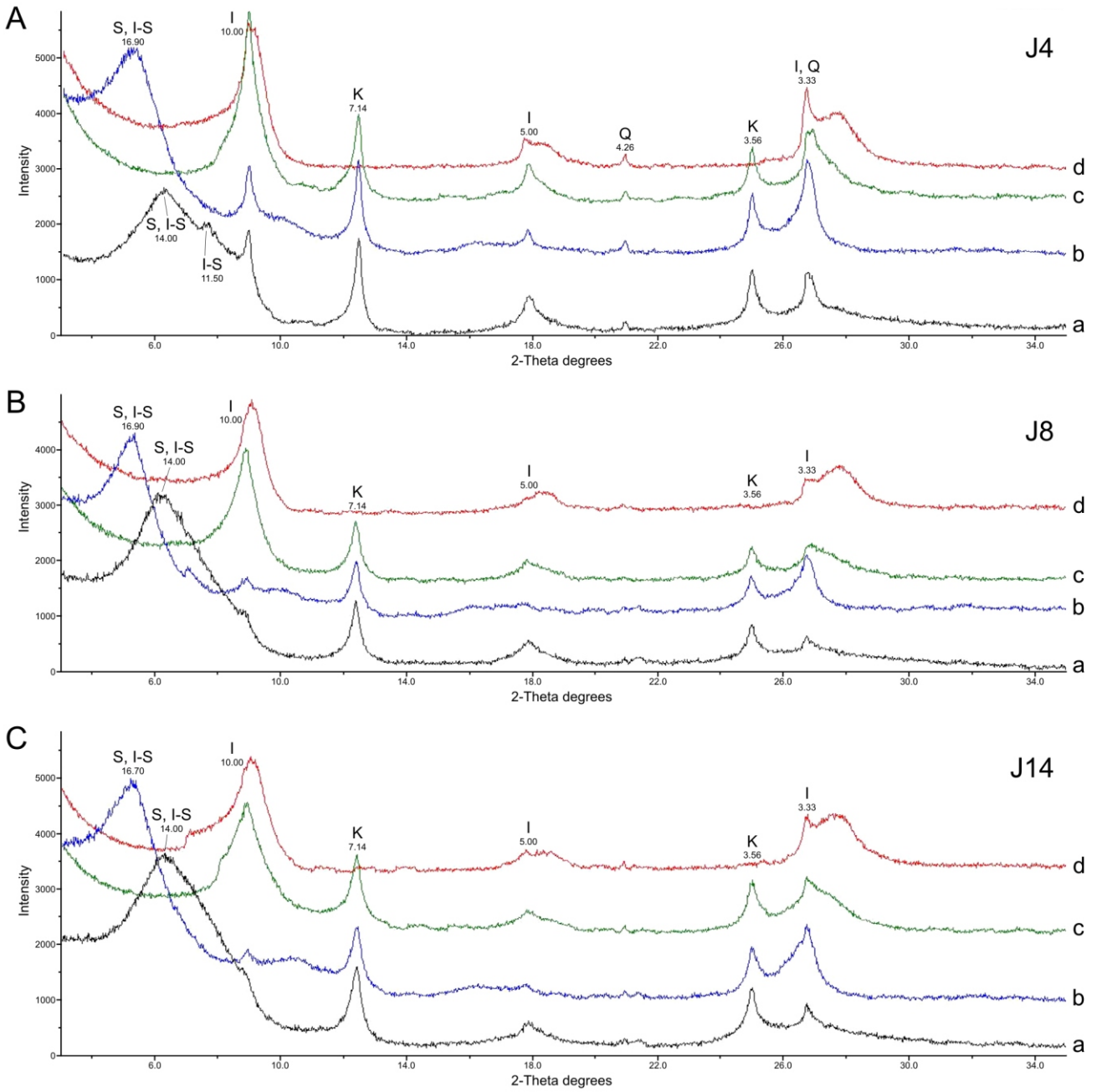

Fig. 5. Powder X-ray diffraction (PXRD) patterns for the clay fraction of representative multi-coloured "Poznań Clays" from the Jóźwin IIB opencast mine

A – sample J4; **B** – sample J8; **C** – sample J14; abbreviations: I-S – "illite"-smectite mixed-layer mineral, I – "illite", K – kaolinite, Q – quartz; prepared samples: a – air-dried, oriented, b – glycolated, c – heated at 350°C, d – heated at 550°C; for colours of the samples analysed (J4, J8, J14), see Figures 1, 3 and Table 1

POWDER X-RAY DIFFRACTION (PXRD) METHOD

The PXRD method was applied separately to both the bulk samples and the clay fraction. All 14 bulk samples were analysed, while 3 clay samples (J4, J8, J14) with clearly different colours were examined to determine their mineral composition. The PXRD measurements were made at the X-ray Structural Laboratory of the Institute of Geology at the Adam Mickiewicz University in Poznań, Poland. All samples were powdered first and then analysed using a *Thermo Electron ARL X'tra* diffractometer (Bragg-Brentano - mode, 260 mm goniometer radius) equipped with a Cu tube and a solid-state Peltier-cooled detector. Its main measurement parameters were as follows: voltage = 40 kV, amperage = 30 mA and power = 1200 W. The range of measurements in continuous scan mode was from 3 to 35° 2 with a scan speed of 0.6°/min. The measurement time was 2 s at a step of 0.02° 2 . In order to improve the randomness of the grain orientation in the X-ray beam, the samples analysed were rotated during the measurements.

The clay fraction (<2 μm) was analysed for samples J4, J8 and J14, characterised by different colours. In general, the research methodology was in line with the recommendations of Moore and Reynolds (1997) and Środoń et al. (2001). Thus, to

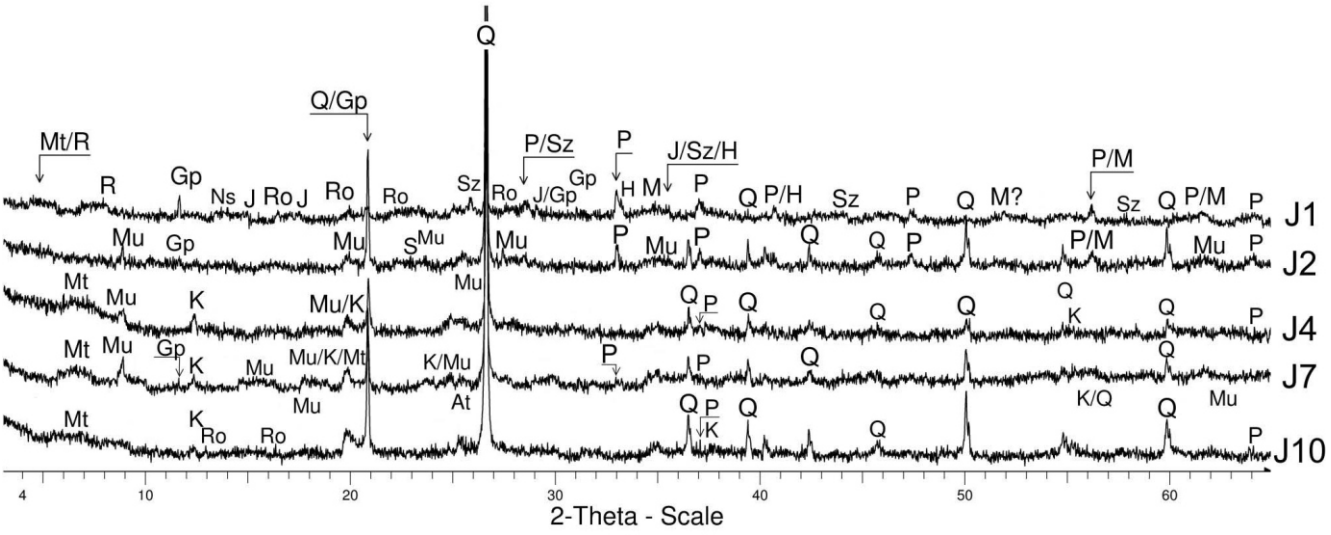

Fig. 6. Powder X-ray diffraction (PXRD) patterns of bulk samples of the "Poznań Clays" with "cold" colours from the Jóźwin IIB opencast mine

At – anatase, Cp – clinoptilolite-Ca, Gp – gypsum, H – hematite (ultra-trace), J – jarosite, K – kaolinite, M – magnetite (possibly titaniferous), Mt – montmorillonite (smectite group), Mu – muscovite ("illite"), P – pyrite, Q – quartz, R – rectorite ("illite"-smectite), Ro – rozenite, Sz – szomolnokite; for colours of the samples analysed, see Figures 1, 3 and Table 1

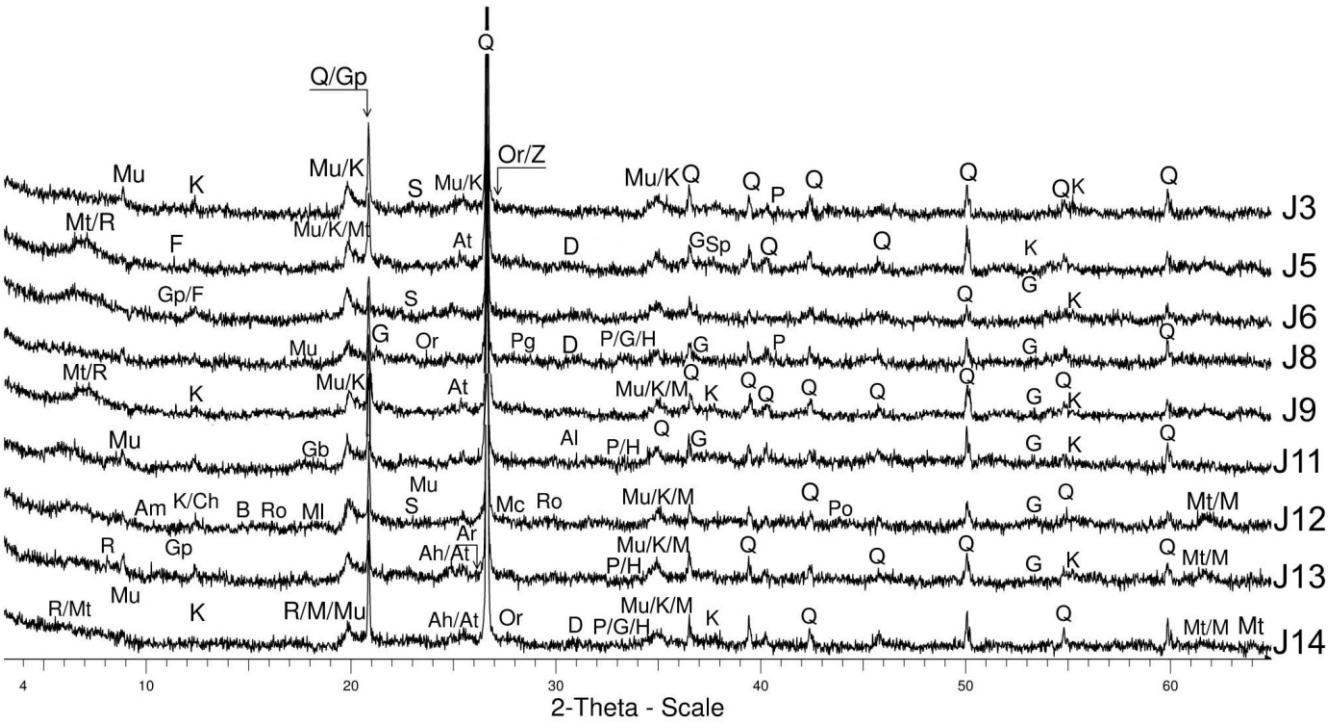

Fig. 7. Powder X-ray diffraction (PXRD) patterns of bulk samples of the "Poznań Clays" with "warm" colours from the Jóźwin IIB opencast

Ch – chlorite, D – dolomite, G – goethite, Ml – melanterite, S – native sulphur, Sp – spinel-group species; for other explanations, see Figure 6

identify the clay minerals, the samples were first air-dried and then treated with ethylene glycol at 60°C for 24 hours; finally, they were heated to 350 and 550°C for 2 hours. This allowed the identification of mixed-layer minerals (i.e., "illite" (muscovite)-smectite, with treatment including glycolation and heating at 350°C) and kaolinite (heated at 550°C). For the bulk samples, such treatment was not required. In this case, the samples were prepared as described by Kruszewski (2013) and Klęsk et al. (2022). The PXRD results of the clay fraction were evaluated using the WinXRD software, while the results of the bulk samples were processed with the *EVA* software of Bruker (Figs. 5–7).

MÖSSBAUER SPECTROSCOPY (^{57}Fe-MS) METHOD

The ^{57}Fe-MS measurements were made at room temperature with a transmission geometry using a *RENON MsAa-4* spectrometer equipped with an LND Inc. Kr-filled proportional detector and a He-Ne laser-based interferometer that was used to calibrate the velocity scale. A commercial ^{57}Co(Rh) source was applied. The source linewidth $_s$ = 0.106(5) mm/s was derived from the fit of the Mössbauer spectrum of 10-μm-thick -Fe foil. Measurements were performed at the Mössbauer Spectroscopy Laboratory of the Pedagogical University in Kraków, Poland.

Mössbauer spectra were fitted using the *MOSGRAF* data processing software suite (Figs. 8, 9 and Table 3). The linewidths reported represent the absorber linewidth $_a$ within the transmission integral approximation, and it can be referred to as the Lorentzian-shaped spectral peak line width with a full width at half maximum (FWHM) that can be assumed to be equal to the following approximation: FWHM = $_a$ + $_s$. The spectral isomer (center) shifts (ISs) are reported with respect to the isomer (centre) shift of room-temperature -Fe. The ^{57}Fe-MS absorbers were prepared using 40 mg/cm^2 of the samples investigated. This test procedure was previously applied by Górnicki et al. (2007) and Błachowski et al. (2008).

Some Fe-bearing minerals have also been identified in this paper as nanocrystals. Their Mössbauer spectra are characterised by a significant broadening of the linewidth $_a$. This is an effect of the superparamagnetic relaxation of electron spins in a magnetic domain of nanoparticles, which depends on the crystallinity (i.e., particle size) as a function of temperature. Thus, it is commonly accepted that the upper size limit for nanocrystals (below which superparamagnetism manifests at room temperature) is ~10 nm (Murad, 2010).

SCANNING ELECTRON MICROSCOPY WITH ENERGY-DISPERSIVE SPECTROSCOPY (SEM-EDS) METHOD

The SEM-EDS method is typically used in conjunction with other methods, such as PXRD, optical microscopy and ^{57}Fe-MS to provide a more comprehensive understanding of geological materials (Goldstein et al., 2017). All samples (J1–J14) were observed and analysed chemically using the SEM-EDS method described above, although only some of them were selected to be shown in this paper (Figs. 10–12). Observations of non-conductive spatial samples were carried out in variable pressure conditions (30 Pa, 20 kV) using magnifications in the range of 130x–1100x.

The samples were examined using an S-3700N Hitachi scanning electron microscope (SEM) coupled with an energy dispersive X-ray spectrometer (EDS) Thermo-Noran SIX microanalyzer. The SEM-EDS analyses were carried out at the

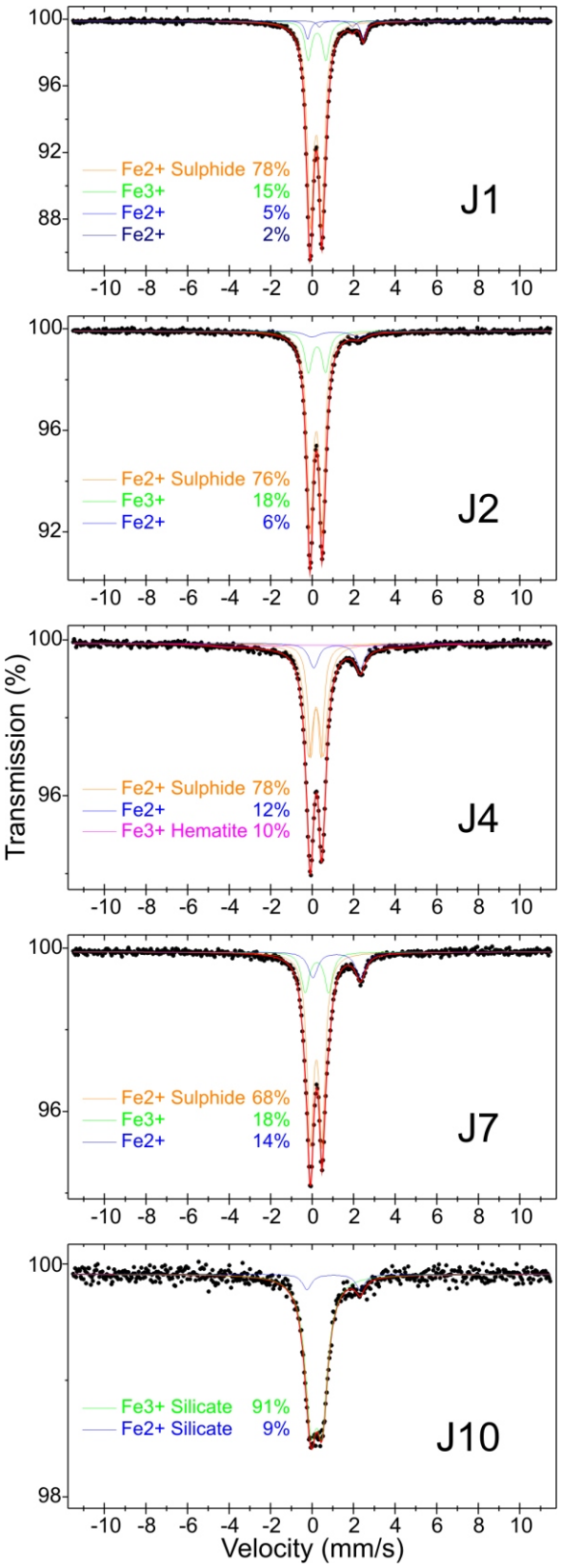

Fig. 8. ^{57}Fe Mössbauer spectra of "Poznań Clays" samples with "cold" colours

The percentages shown correspond to the relative distribution of the Fe atoms into respective iron-bearing minerals; the sample numbers are the same as in Figures 2, 3 and Tables 1–3; for more details of the spectral components, see Table 3

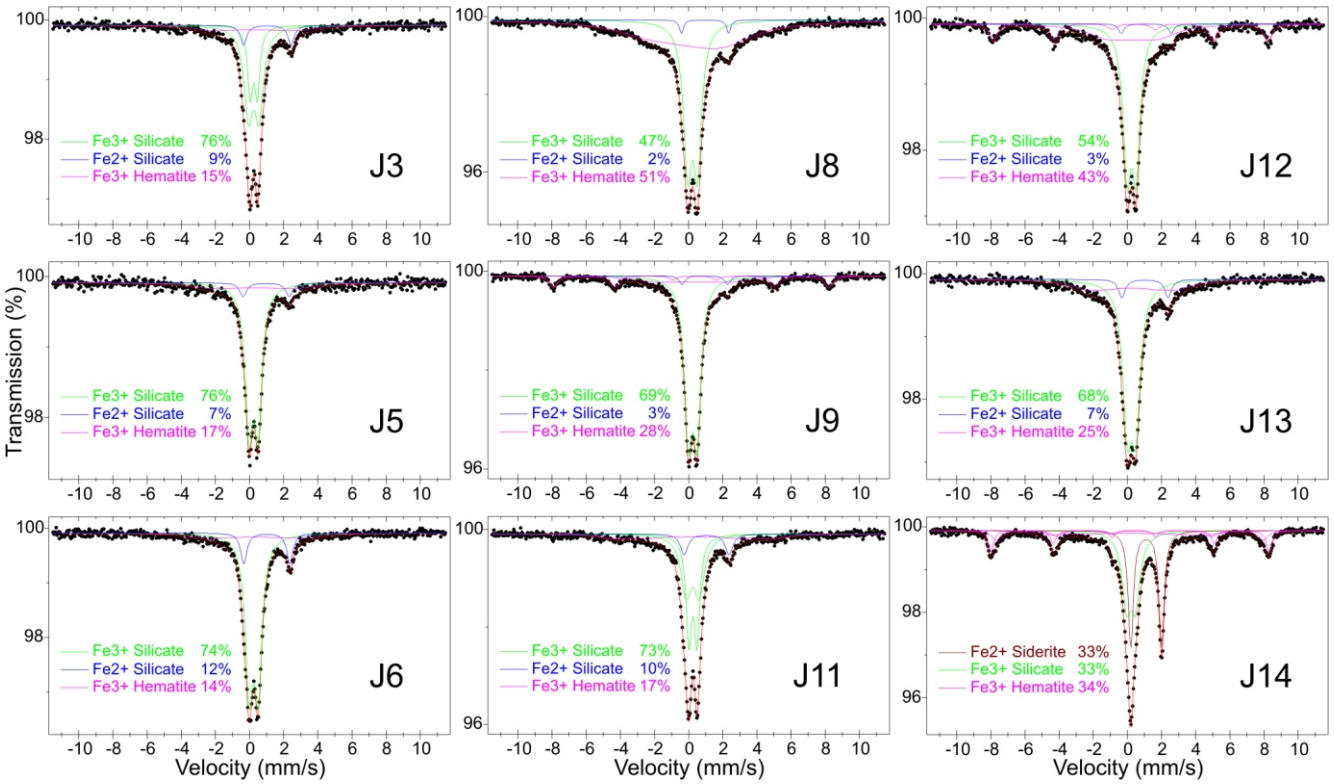

Fig. 9. ^{57}Fe Mössbauer spectra of "Poznań Clays" samples with "warm" colours

Explanations as in **Figure 8**

Laboratory for Scanning Electron Macroscopy and Microanalysis, Faculty of Geographical and Geological Sciences, Adam Mickiewicz University, Poznań, Poland.

RESULTS

MACROSCOPIC AND DIGITISED COLOUR OF THE SEDIMENT

DESCRIPTION OF SECTION AND SEDIMENT COLOUR

The "Poznań Clays" that were studied rest directly on the roof of the lignite seam (MPLS-1). They are glaciotectonically folded, but their continuity is not broken and the original stratigraphy is preserved (Fig. 2A). Within the section examined (~4.7 m thick), 14 layers with different colours were distinguished. The lowest dark grey bed is 30 cm thick and is characterised by macroscopically visible dispersed organic particles and xylites (i.e., fossilised pieces of wood >1 cm in size). In sample J1, the organic matter is clearly visible, while in sample J10, the organics are very finely dispersed, as confirmed by H_2O_2.

INTERPRETATION

The remaining strata are composed of alternating sediments of "warm" (yellow, orange, cherry-red, red) and "cold" (greyish blue, greyish violet, green) colours. These colours appear different and have other names for air-dried, dry and powdered samples, and they depend on the colour description used, that is, the Munsell system or the RGB system (cf. Figs. 2B, C, 3 and Table 1).

GRAIN SIZE OF THE SEDIMENT

DESCRIPTION OF FRACTION

Among the samples tested, only sample J6 represents clay; most of the samples (8 of 14) are silty loam. In the second case, no sample can be classified as clay. As many as 9 samples are silts, and the remaining 5 samples represent clayey silt (J4, J5, J9, J10) and silty clay (J6), respectively (Fig. 4 and Table 2).

INTERPRETATION

In this paper, the term "clays" is put in quotation marks because the sediments investigated are not actually clays. This statement is true for the USDA (Retallack, 2019) and Shepard (1954) classifications as described above.

MINERAL COMPOSITION OF THE SAMPLES ANALYSED

MINERALOGY OF THE CLAY FRACTION

DESCRIPTION OF CLAY MINERALS

The mineral compositions of the clay fractions (<2 μm) of three selected multi-coloured samples (J4, J8, J14) are very similar (Fig. 5). A mixture of swelling minerals such as smectite (S) and "illite"-smectite (I-S) (hereinafter referred to as rectorite) predominate in the material analysed, as seen from their broad peaks. This is shown by a shift in the peak positions from ~14 Å (air-dried) to ~17 Å (glycolated), which indicates a significant

Table 3

^{57}Fe Mössbauer spectroscopy parameters of "Poznań Clays" samples from the Jóźwin IIB opencast mine (Konin Lignite Mine, central Poland)

Sample number	Fe-bearing phase	A [%]	IS [mm/s]	QS [mm/s]	$_a$ [mm/s]	*B* [Tesla]
J1	Fe2+: sulphide	78	0.30	0.55	0.24	–
	Fe3+: ferrihydrite?	15	0.35	0.86	0.27	–
	Fe2+: hydrous sulphate?	5	1.23	2.67	0.18	–
	Fe2+: hydrous sulphate?	2	1.26	1.59	0.22	–
J2	Fe2+: sulphide	76	0.30	0.57	0.23	–
	Fe3+: ferrihydrite?	18	0.35	0.83	0.31	–
	Fe2+: hydrous sulphate?	6	1.23	2.27	0.73	–
J3	Fe3+: silicate	24	0.36	0.42	0.26	–
	Fe3+: silicate	52	0.36	0.62	0.53	–
	Fe2+: silicate	9	1.15	2.78	0.34	–
	Fe3+: nano-hematite?	15	0.38	–	2.0	17
J4	Fe2+: sulphide	32	0.29	0.50	0.23	–
	Fe2+: sulphide?	46	0.30	0.71	0.39	–
	Fe2+: hydrous sulphate?	12	1.31	2.25	0.44	–
	Fe3+: nano-hematite?	10	0.38	–	2.0	27
J5	Fe3+: silicate	76	0.35	0.53	0.43	–
	Fe2+: silicate	7	1.08	2.69	0.37	–
	Fe3+: nano-hematite?	17	0.35	–	2.0	16
J6	Fe3+: silicate	74	0.36	0.53	0.44	–
	Fe2+: silicate	12	1.12	2.69	0.32	–
	Fe3+: nano-hematite?	14	0.36	–	2.5	18
J7	Fe2+: sulphide	68	0.31	0.57	0.27	–
	Fe3+: jarosite?	18	0.34	1.13	0.35	–
	Fe2+: hydrous sulphate?	14	1.29	2.29	0.45	–
J8	Fe3+: silicate	47	0.35	0.57	0.48	–
	Fe2+: silicate	2	1.08	2.76	0.19	–
	Fe3+: nano-hematite?	51	0.4	–	4	14
J9	Fe3+: silicate	69	0.35	0.51	0.44	–
	Fe2+: silicate	3	1.06	2.66	0.3	–
	Fe3+: hematite	13	0.36	–0.20	0.49	50.0
	Fe3+: nano-hematite?	15	0.36	–	2.5	16
J10	Fe3+: silicate	91	0.33	0.54	0.56	–
	Fe2+: silicate	9	1.15	2.56	0.42	–
J11	Fe3+: silicate	36	0.36	0.48	0.29	–
	Fe3+: silicate	37	0.34	0.76	0.63	–
	Fe2+: silicate	10	1.16	2.63	0.44	–
	Fe3+: nano-hematite?	17	0.38	–	2.0	28
J12	Fe3+: silicate	54	0.36	0.53	0.45	–
	Fe2+: silicate	3	1.21	2.92	0.3	–
	Fe3+: hematite	16	0.39	–0.17	0.46	49.9
	Fe3+: nano-hematite?	27	0.39	–	2.5	11
J13	Fe3+: silicate	68	0.35	0.50	0.53	–
	Fe2+: silicate	7	1.14	2.71	0.37	–
	Fe3+: nano-hematite?	25	0.35	–	2.0	17
J14	Fe2+: siderite?	33	1.21	1.81	0.26	–
	Fe3+: silicate	33	0.32	0.52	0.54	–
	Fe3+: hematite	12	0.37	–0.23	0.28	50.5
	Fe3+: hematite	10	0.37	–0.23	0.57	48.5
	Fe3+: nano-hematite?	12	0.37	–0.23	2.0	28

A – relative area of respective spectral component (distribution of Fe atoms into respective Fe-bearing minerals), IS – isomer (centre) shift relative to room temperature -Fe, QS – quadrupole splitting, $_a$ – absorber line-width (within transmission integral approximation), *B* – hyperfine magnetic field; errors are of the order of unity for the last digit shown; the sample numbers are the same as in Figures 2, 3, 6–9 and Tables 1, 2

amount of S and I-S, and these peaks turn into a “saddle” at 350°C. Among the clay minerals, in addition to S and I-S, “illite” (I) and kaolinite (K) were found. The following reflections are characteristic of “illite”: ~10.5 and 3.33 Å. The stable positions of the reflections at 7.14 and 3.56 Å (in air-dried, glycolated and heated samples), on the other hand, indicate kaolinite. This convincingly confirms the disappearance of both peaks in the material heated to 550°C. Additionally, in sample J4, traces of quartz (Q) were found—the values of the respective peaks are 4.24 and 2.33 Å. This sample (J4) also has a relatively higher “illite” content compared to samples J8 and J14 (Fig. 5).

INTERPRETATION

The results concerning the minerals in the clay fraction are consistent with those obtained in other studies of the “Poznań Clays” (cf. Górniak et al., 2001; Duczmal-Czernikiewicz, 2010, 2013). Nevertheless, taking into account the difficulties of quantitative analysis of mixed-layer clay minerals, as described by Środoń (1999) and Środoń et al. (2001), the shape of the interpreted PXRD peaks and their positions are almost identical (see Fig. 5). This means that the qualitative compositions of the clay minerals in the samples being compared (J4, J8, J14) are very similar. Thus, the clay minerals contained in the “Poznań Clays” are not decisive in determining their main colour. This question is discussed in more detail below.

MINERALOGY OF THE BULK SAMPLES

DESCRIPTION OF ALL MINERALS

Powder X-ray diffraction, as a method that is very sensitive to phase composition changes (i.e., with detection limit <0.n wt.%; TCMS, 2022), made it possible to constrain variations in the mineral composition of the samples studied. Quartz and, to a much lesser extent, gypsum are the dominant components in all samples of both “cold” and “warm” colours examined. The clay minerals described and interpreted above are also present in these samples. On the X-ray graphs of bulk samples, clay minerals are mainly classified as rectorite (interstratified species of “illite”-smectite type; barycenter at 13.6 Å), smectite-group species (herein referred to as smectite, d = 15 Å) and possible traces of halloysite (7 Å polytype, e.g., d = 4.43 Å). However, kaolinite and “illite” (described as muscovite in Figs. 6 and 7) were also found in all samples representing the “Poznań Clays” (cf. Figs. 5–7).

INTERPRETATION

A common feature of the “cold”-coloured samples is the presence of gypsum and pyrite, except for sample J10 (Fig. 6). The content of other minerals varies from sample to sample. Some minerals occur only in trace amounts, while the presence of other minerals is uncertain. Sample J1, for example, has elevated amounts of the products of pyrite weathering, namely the sulphates szomolnokite (d = 2.94 and 4.004 Å) and rozenite. It also contains trace amounts of jarosite, goethite and magnetite (possibly titaniferous). The remaining “cold”-coloured samples are less mineralogically diverse, although they contain minerals that differentiate them. Sample J2 contains traces of magnetite, while sample J4 is characterised by a small amount of plagioclase and ankerite/dolomite. Clinoptilolite (d = 8.89 Å), anatase (d = 3.52 Å) and the fougèrite group species – FGS (d = 7.81 Å) were identified in sample J7.

The “warm”-coloured samples generally have mineral compositions similar to those described above, that is, they are dominated by quartz and to a lesser extent by gypsum, and among the clay minerals, smectite, “illite”-smectite (rectorite), kaolinite and “illite” (cf. Figs. 5–8) are present. Samples J3, J5 and J9 are the only samples in which sulphur was found using the PXRD method. In the last case, an admixture of anatase (d = 3.52 and 1.70 Å) is typical of this sample. Nevertheless, the most important feature of sample J5 in terms of its mineralogical chromophores is its pronounced FGS content. The presence of the FGS is indicated by a very sharp reflection at 7.81 Å. Sample J8 is the most goethite-rich sample, although tiny amounts of pyrite and hematite are also possible (Fig. 7). Traces of pyrite and hematite are evident in sample J11. Magnetite occurs in samples J12–J14, while the presence of goethite is less evident. By contrast, dolomite was found in sample J14 (Fig. 7).

^{57}FE MÖSSBAUER SPECTROSCOPY

DESCRIPTION OF IRON VALENCE

Like the PXRD results, the ^{57}Fe-MS results were also divided into two groups corresponding to the “cold” and “warm” colours of the samples studied (Figs. 8 and 9). Most of these samples (J1, J2, J4, J7) are characterised by the predominance of sulphide (68–78% of all iron atoms contained in a particular sample), i.e., pyrite, which is also corroborated by the PXRD and SEM-EDS results (cf. Figs. 6, 8 and 10). The rest of the ferrous and ferric iron cations (Fe^{2+}, Fe^{3+}) may be found in ferrihydrite, hydrous sulphate (jarosite, as shown by PXRD in sample J1), silicates and trace amounts of nano-hematite in sample J4 (Table 3). In this group, sample J10 is an exception; in this sample, Fe was found only in silicates, that is, in clay minerals (cf. Figs. 5 and 8); this sample (J10) contains organic matter on a micro-scale and traces of anatase (see Fig. 6).

INTERPRETATION

“Warm”-coloured samples share two common characteristics. First, Fe^{3+}-rich silicates containing Fe^{3+} ions predominate in most of the samples; second, almost all samples of this colour group contain hematite or goethite (Fig. 9). Among them the third component is Fe^{2+}-rich silicate, but in smaller amounts that range from 2 to 12% of all iron atoms. As the results of the ^{57}Fe-MS method clearly show, sample J14 (red in colour, 10R 5/4) differs from the other samples in terms of the composition of iron minerals, as it probably contains other mineral(s) such as siderite (although this was not confirmed by PXRD and SEM-EDS) and does not contain Fe^{2+}-rich silicate (Fig. 9 and Table 3).

MINERALS IDENTIFIED BY SEM-EDS

DESCRIPTION OF THE MAIN MINERAL COMPONENTS

Considering the PXRD and ^{57}Fe-MS results, we additionally identified some of the minerals that directly or indirectly affect the colour of the “Poznań Clays” examined using the SEM-ESD method. In “cold”-coloured sediments, except for sample J1, which contains jarosite, there are no potentially strong pigments (hematite, goethite, jarosite; cf. Klęsk et al., 2022; Klęsk, 2023), while framboidal and weathered pyrite, and well-crystallised gypsum and/or native sulphur are present (Fig. 10).

Microscale organic matter was found (sample J4; Fig. 10C), also in samples J2, J7 and J10. The exception here is sample J1; in this sample, organic macroremains (e.g., twigs, rootlets, stems) and strongly coalified plant detritus were identified in the field, in the Jóźwin IIB lignite opencast mine.

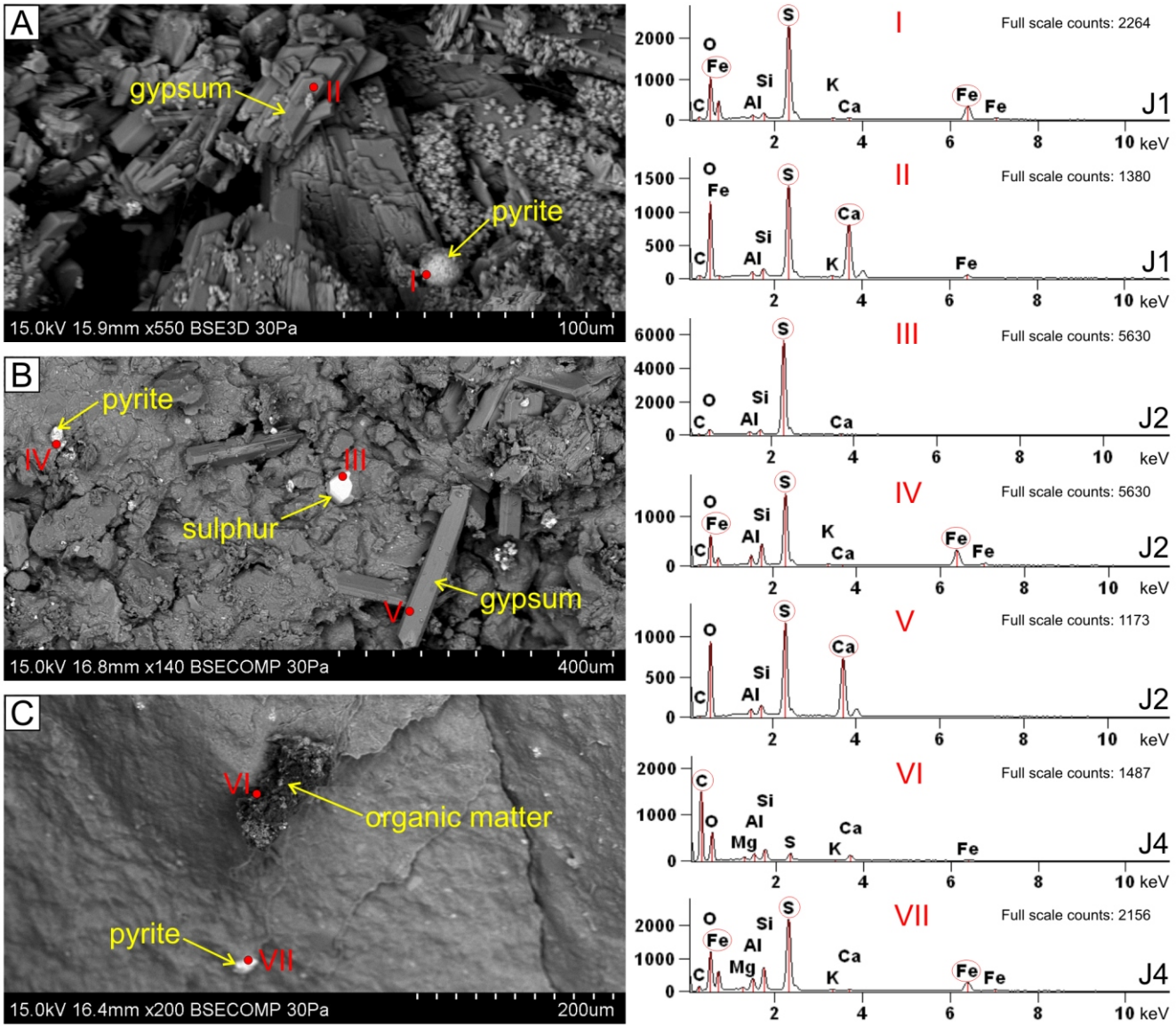

Fig. 10. Representative SEM photographs of "Poznań Clays" samples with "cold" colours and EDS spectrograms depicting local elemental composition (I–VII)

Dominant elements are outlined in red

Sediments with "warm" colours contain hematite or goethite (not identified convincingly in this study by SEM-EDS) as the main colouring pigments. These samples occasionally contain only traces of pyrite. Well-crystallised sulphur is also present; for example, it was identified in sample J3 (Fig. 11B). On the other hand, hematite in various grain sizes, forms and degrees of weathering, as the main (except for goethite) pigment of "warm"-coloured sediment, was found in samples J13 and J14 (Fig. 11B–D).

As an example, for sample J14, using SEM-EDS, the surface distribution of iron as the primary colour carrier in the sediments is demonstrated (Fig. 12). The Fe distribution is very uneven, Fe being almost absent in the lower left corner and in the upper left part of this sample (Fig. 12B).

INTERPRETATION

The surface analysed includes <5 vol.% and <10 wt% of Fe (Fig. 12C). Its distribution determines the colour of the "Poznań Clays" and the presence of mottles in them. If trivalent iron predominates, as in the case of samples J3, J5, J6, J8, J9 and J11–J14 (cf. Fig. 9 and Table 3), these mottles are larger and redder, both on a micro- and macro-scale, giving the sediment a "warm" colour. However, the presence of hematite and/or goethite was not confirmed by PXRD in samples J3 and J9, probably due to the content of these minerals being below the detection limit (see Fig. 7) or large Scherrer widening, which is especially well-known for goethite (e.g., Nørlung Christensen et al., 2007). The latter phenomenon can cause reflections of finely crystalline phases to be "lost" within the background.

DISCUSSION

WHICH COMPONENTS DETERMINE THE SEDIMENT COLOUR?

The PXRD results obtained for the clay fraction from the "Poznań Clays" indicate their similar mineral compositions. Simply put, the varicoloured sediments examined consist primarily of smectite and "illite"-smectite (rectorite), accompanied

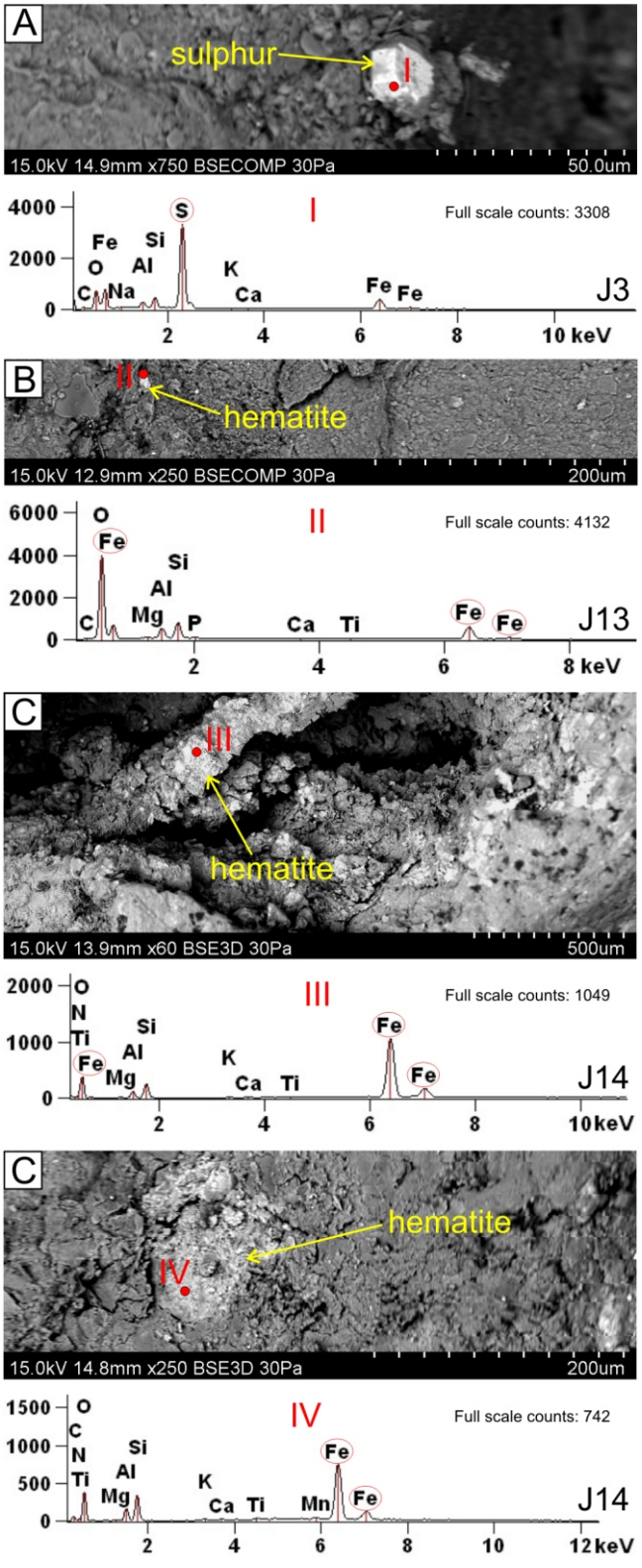

Fig. 11. Representative SEM photographs of the "Poznań Clays" samples with "warm" colours and EDS spectrograms depicting local elemental composition (I–IV)

Explanations as in Figure 10

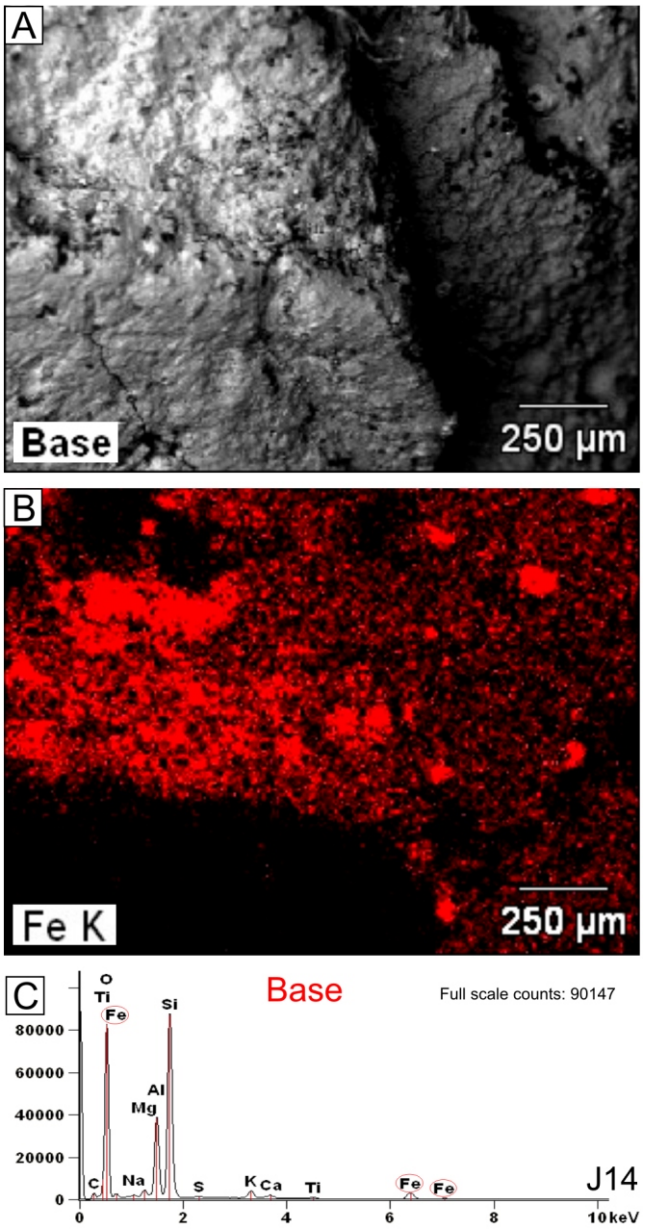

Fig. 12. Surface distribution of iron in sample J14

A – general SEM image; **B** – map of iron distribution; **C** – EDS spectrogram depicting the elemental composition of the area shown in Figure 12A, B

by "illite" and kaolinite (see Fig. 5). This is consistent with other results for the "Poznań Clays" from different areas of the sedimentary basin (Wiewióra and Wyrwicki, 1974; Wyrwicki, 1975; Choma-Moryl, 1988; Górniak et al., 2001; Widera, 2007; Bojakowska et al., 2010; Duczmal-Czernikiewicz, 2010, 2013).

Nevertheless, an increased amount of "illite" (containing Fe^{2+}) may give the sediment a greenish shade when the ratio of Fe^{3+}/Fe^{2+} is very low (Myrow, 1990, 2003); this type of "illite" is referred to as green "illite" (McBride, 1974). This occurs in sample J4, which has the highest fraction of sulphides (78% of all Fe cations), namely pyrite; this indicates reducing conditions that favoured the transformation of an Fe-rich smectite structure into a more "illite"-like structure by bacterial action (Petit et al., 2017). The colour of these minerals in aqueous suspension

Table 4

Typical colours of minerals identified in the samples studied and colours of their powders (streak) (according to Mindat, 2022)

Species	Formula	Colour	Streak colour
anatase	TiO_2	variable (including dark blue-grey)	white to yellowish
feroxyhyte	$Fe^{3+}O(OH)$	yellow-brown, brown	yellow
ferrihydrite	$Fe^{3+}_{10}O_{14}(OH)_2$	dark brown, yellow-brown	yellow-brown
glauconite	$(K,Na)(Fe^{3+},Al,Mg)_2(Si,Al)_4O_{10}(OH)_2$	*blue-green, green, yellow-green*	light green
goethite	Fe^{3+}**O(OH)**	brownish black, yellow-brown, reddish brown	yellowish brown, orange-yellow, reddish brown
hematite	Fe^{3+}_2**O**$_3$	grey, red	red, brownish red
magnetite	Fe^{2+}**Fe**$^{3+}_2$**O**$_4$	black	black
melanterite	$Fe^{2+}SO_4 \cdot 7H_2O$	blue-green	white
pyrite	Fe^{2+}**S**$_2$	pale brass-yellow	greenish-black
szomolnokite	$Fe^{2+}SO_4 \cdot H_2O$	variable (mostly yellowish)	white

The main minerals that affect the sediment colour are in bold; trace or questionable minerals that may affect the sediment colour are in italics

changes from yellow to green, blue-green and blue-grey (Stucki, 2011). However, in a natural environment (that also contains other minerals discussed below), only some of the Fe^{3+} turns into Fe^{2+}, which may give the sediment yellow-greenish to bluish shades, as described in the field (see Table 1). In conclusion, taking into account all available information, it can be unequivocally stated that clay minerals do not determine the main colour of the "Poznań Clays" investigated, but these minerals may affect the shade of the "Poznań Clays." This statement is consistent with the results of Nemec and Porębski (1977) for Permian deposits from SW Poland.

Apart from organic matter, only five minerals determine the colour of the deposits studied. These are hematite, goethite, jarosite, the weathered (partially converted to other pigments) remains of pyrite, and probably magnetite if present. Only the first two play a significant role in "warm"-coloured samples. The "warm" colour of jarosite is completely overprinted by organic matter in sample J1, which is dark grey to black (cf. Figs. 1, 2, 6 and Table 1). Magnetite, if present in larger amounts, would give the sediment a blackish colour, while pyrite is primarily common in cold-coloured samples, indicating reducing conditions (e.g., PiPujol and Buurman, 1994; Ratajczak et al., 2015; Muslim and Ritung, 2021). Of other secondary minerals, mainly those containing trivalent iron, can give the sediment a "warm" shade. These include feroxyhyte and ferrihydrite, as well as szomolnokite, which contains divalent iron (Table 4). However, due to the trace amounts of these minerals, sometimes at the limit of detection, their presence can only enhance the "warm" colour of some layers of the "Poznań Clays."

Explanations for the "cold colours" of the sediments studied are more complex. The FGS belong to the hydrotalcite supergroup (Mills et al., 2012), and its compounds are known as double-layered hydroxides, such as ferrihydrite and feroxyhyte (Table 4). Ferrihydrite is recognised as the precursor of the FGS under reducing conditions. It is metastable and can therefore easily decompose into magnetite at 30 °C. Moreover, the oxidation of such FGS leads to the formation of another typical soil mineral, that is, lepidocrocite. In the case of feroxyhyte, it is also indicated by gleyed soil horizons that are termed gleysoils (Mills et al., 2012).

Under appropriate redox conditions, carbonate-rich FGS can yield goethite, while sulphate-rich FGS can transform into both goethite and lepidocrocite (Johnson, 2014; Zhitova et al., 2016; Srivastava et al., 2021; Misol et al., 2022). Therefore, taking into account the fluvial origin of the "Poznań Clays" and the reflection position (Figs. 6 and 7; samples J7 and J5, respectively), we believe that the anatase and melanterite detected may give the sediment a bluish to greenish shade, if they were more common and present in significantly greater amounts (Table 4). In the latter case, a suitable finer fraction would also be necessary to induce the colour.

From the results obtained using ^{57}Fe-MS, the main colouring agent in "Poznań Clays" from the Jóźwin IIB lignite opencast is hematite. However, its presence is not always certain, especially in the case of nano-hematite (see Table 3). Our main purpose here was not to identify mineral phases, but to precisely determine the valency of the iron contained in them. In the "cold"-coloured layers, the lack of hematite or its traces (up to 10%, sample J4), and in the absence of other pigment minerals, gives the sediment a grey colour. A higher or lower content of organic matter (samples J1 and J10) gives the sediment a darker or paler shade, respectively (cf. Myrow, 1990). Other shades from greenish to bluish (samples J2, J4, J7, J10), as well as the influence of organic matter on the sediment colour, cannot be investigated by the ^{57}Fe-MS method.

The best evidence comes from silicates, mainly clay minerals, but the differentiation of silicates using the ^{57}Fe-MS method is uncertain (Murad and Cashin, 2004; Stevens et al., 2005; Dyar et al., 2006; Murad, 2010). In brief, the greenish-bluish shades may come from a relatively higher "illite" content (sample J4; see Fig. 5), from trace amounts of some pigments such as anatase (sample J10; see Fig. 6) and/or from the presence of fine-grained pyrite, indicative of reducing conditions in the sediment (Rickard and Luther, 2005, 2007; Ratajczak et al., 2015), as determined by PXRD and SEM-EDS analysis (cf. Figs. 6 and 10). Pyrite is very common in ancient (e.g., PiPujol and Buurman, 1994; Retallack, 2019) and modern hydromorphic soils (e.g., Muslim and Ritung, 2021).

By contrast with the "cold" colours, the remaining samples owe their "warm" colours mainly to hematite and goethite. However, the differences between the colours do not directly depend on their content; they also depend on the content and composition of other minerals, including those that do not contain Fe cations (see Fig. 7). In the case of iron-bearing minerals, in all samples with "warm" colours examined, the Fe^{3+}/Fe^{2+} ratio is always many times greater than 1, that is, between ~2 (sample J14) and 49 (sample J8; cf. Fig. 9 and Table 3). Otherwise, native sulphur crystals, which are often associated with gypsum, may give the sediment a yellowish shade; their presence was shown by PXRD and SEM-EDS (cf. Figs. 6, 7, 10B and 11A).

There exist “marine red beds” (MRBs), which received their colour during deposition and early diagenesis at specific redox values as a response to changes in geochemical conditions and biological activities. Studies of MRBs use some of the same methods as we used in the current study, but they are mainly based on rock geochemistry and/or the carbon isotopic composition (^{13}C) (e.g., Neuhuber et al., 2007; Song et al., 2017; Bábek et al., 2021, 2022; Card and Montenari, 2023). Nevertheless, the results obtained for the MRBs in the studies cited are consistent with those for terrigenous sediments (e.g., Nemec and Porębski, 1977; Torrent et al., 1980; Cornell and Schwertmann, 2003; Srivastava et al., 2013; Retallack, 2019; Upreti and Srivastava, 2019), including the majority of the “warm”-coloured deposits investigated in this paper.

In both of the environments mentioned (i.e., marine and terrestrial), hematite (-Fe_2O_3) and goethite (-FeOOH), which is often transformed into hematite, are considered to be the dominant mineral pigments. In the case of hematite, this statement is true not only for conditions prevailing on Earth but also on the surface of Mars (e.g., Jiang et al., 2022). However, there is another candidate: macaulayite, $(Fe,Al)_{24}Si_4O_{43}(OH)_2$, which is a swelling phyllosilicate that is very rare on Earth but has been suggested to likely occur on Mars (Hillier/NASA, vide Bishop, 2009). Goethite forms under acid weathering conditions (pH of ~5) in sediment in poorly drained environments, while hematite formation requires a neutral pH (~7–8) and well-drained conditions. Additionally, progressive aridity of the climate (discussed below) is more favourable for the creation and preservation of hematite than for goethite (e.g., Schwertmann, 1985, 1993; Kraus and Riggins, 2007; Colombo et al., 2016; Spinola et al., 2018).

FORMATION OF MULTI-COLOURED SEDIMENTS

The “Poznań Clays” began to accumulate when deposition of the underlying lignite seam (MPLS-1) terminated, that is, at ~14.3 Ma (Widera et al., 2021a, 2023). However, the end of the formation of the “Poznań Clays” can only be loosely estimated at the earliest Pliocene (~5.0 Ma; Troć and Sadowska, 2006; Widera et al., 2021b) due to the erosion of their uppermost layers in the Pleistocene. The lower unit of the “Poznań Clays” (i.e., “grey clays,” uppermost Grey Clays Member, lower Poznań Formation; sample J1 with dispersed organic matter and xylites) is interpreted as being deposited at the final stage of the MPLS-1 accumulation from 14.3–13.8 Ma. Simply put, the “grey clays” were deposited in shallow lakes located on top of Mid-Miocene mires (Piwocki and Ziembińska-Tworzydło, 1997; Piwocki et al., 2004). Then, after 13.8 Ma, the “green clays” and the “flame-like clays” (Wielkopolska Member, upper Poznań Formation; samples J2–J14) began to accumulate in the overbank zones of the upper Neogene anastomosing or anastomosing-to-meandering river systems (Maciaszek et al., 2019, 2020; Widera et al., 2019; 2021a, b; Zieliński and Widera, 2020).

The deposition of the “Poznań Clays” in central Poland depended on the overlapping of both global and regional tectonic and palaeogeographic processes. The “grey clays” formed from 0.7–1.2 Ma after the Mid-Miocene Climatic Optimum, which occurred around 15 Ma (Zachos et al., 2001). At that time, the climate began to cool and dry. This process was relatively slow at first, but around 13.8 Ma (the beginning of the Badenian Salinity Crisis in the Carpathian Foredeep), there was an abrupt drop in temperature and rainfall in the study area. Under the conditions of progressive cooling, drying and seasonality (Kasiński and Słodkowska, 2016; Widera et al., 2021b), the majority of the “Poznań Clays” (“green clays” and “flame-like clays”) accumulated in one or more endorheic “terminal floodplain” basins (Widera, 2013; Widera et al., 2017, 2019; Maciaszek et al., 2019).

The overbank (extra-channel) areas, where the investigated “Poznań Clays” were deposited, were generally well drained, resulting in Vertisols with “warm” colours. However, due to uneven vertical tectonic movements and compaction of the underlying lignite-bearing deposits, some overbank zones were poorly drained for varying lengths of time; this resulted in hydromorphic palaeosols with “cold” colours, including the Histosols. The complex nature of many palaeosol horizons with “cold” colours may indicate that they may have undergone a secondary gleyed stage (PiPujol and Buurman, 1994; Kraus, 1999; Retallack, 2019). However, isochronous and lateral changes in sediment colour are even more common than relatively long-term climatic fluctuations. This may reflect the morphology of the overbank zone and the distance from the adjacent river channels (Bown and Kraus, 1981, 1987). In summary, it can be stated that the colours of the “Poznań Clays” depend on the redox conditions that prevailed during or shortly after their accumulation on the floodplains, as corroborated by our results as described above.

CONCLUSIONS

1. PXRD, ^{57}Fe-MS and SEM-EDS techniques were applied to explain the different colours of the “Poznań Clays” (upper Neogene, Polish Lowlands). These multi-coloured deposits have been considered to be terrestrial in recent years. From a sedimentological point of view, their fluvial origin is indicated by, among other things, the presence of river palaeochannels and palaeosol horizons, including thin lignite layers (see the Appendix). PXRD was used to identify minerals, ^{57}Fe-MS made it possible to quantify the content of divalent and trivalent iron and SEM-EDS analysis provided images of some of the major minerals and estimated their chemical compositions.

2. We have corroborated earlier findings that hematite and/or goethite (or a lack of them) are the main colouring mineral pigments. In outline, layers with “cold” colours do not contain hematite/goethite or contain only traces of these minerals, while those with “warm” colours are relatively rich in hematite and/or goethite. Other factors also influence the hues of the sediments. The most important of these factors is the presence of native sulphur (“warm” colours), pyrite, anatase, green “illite,” possibly also minerals belonging to the fougèrite group species (FGS) and, most of all, organic matter (“cold” colours). The quartz and gypsum present in all samples analysed do not affect their colour and the shade.

3. Differences in the colour of the “Poznań Clays” may be linked with both global and regional climate changes, as well as with local floodplain morphology and location in relation to the upper Neogene fluvial palaeochannels. Under conditions of progressive cooling, drying and the seasonality of the climate, and on elevations of the floodplain, Vertisols (“warm” colour, rich in hematite and/or goethite) could develop. By contrast, after floods and in the floodplain depressions, below the groundwater table, there were favourable conditions for the formation of hydromorphic soils (with “cold” colours, rich in pyrite and always containing organic matter), including Histosols.

Acknowledgements. The authors would like to thank P. Szymura (Department of Geomorphology, Adam Mickiewicz University in Poznań, Poland) for carrying out the grain-size analysis by laser diffraction. We are grateful to M. Kubiak for help with the PXRD analysis (Institute of Geology, Adam Mickiewicz University in Poznań, Poland). We also express our deep appreciation to both reviewers for suggestions which greatly improved our manuscript.

REFERENCES

Areń, B., 1964. Atlas geologiczny Polski. Zagadnienia stratygraficzno-facjalne. Trzeciorzęd (in Polish), 11/a. Wyd. Geol., Warszawa.

Bábek, O., Vodrážková, S., Kumpan, T., Kalvoda, J., Holá, M., Ackerman, L., 2021. Geochemical record of the subsurface redox gradient in marine red beds: a case study from the Devonian Prague Basin, Czechia. Sedimentology, **68**: 3523–3548; https://doi.org/ 10.1111/sed.12910

Bábek, O., Kumpan, T., Li, W., Holá, M., Šimíček, D., Kapusta, J., 2022. Incipient reddening of Ordovician carbonates: The origin and geochemistry of yellow and pink colouration in limestones. Sedimentary Geology, **440**: 106262; https://doi.org/ 10.1016/j.sedgeo.2022.106262

Badura, J., Przybylski, B., 2004. Evolution of the Late Neogene and Eopleistocene fluvial system in the foreland of the Sudetes Mountains, SW Poland. Annales Societatis Geologorum Poloniae, **74**: 43–61.

Bishop, L., 2009. Rare Scottish mineral may indicate life on Mars; https://phys.org/news/2009-12-rare-scottish-mineral-life-mars.html (retrieved on 15.02.2023)

Błachowski, A., Ruebenbauer, K., Żukrowski, J., Górnicki, R., 2008. Early design stage of the MsAa-4 Mössbauer spectrometer. Acta Physica Polonica A, **114**: 1707–1713; https://doi.org/10.12693/APhysPolA.114.1707

Bojakowska, I., Barański, P., Iwasińska-Budzyk, I., Retka, J., 2010. Zróżnicowanie zawartości pierwiastków śladowych w iłach poznańskich (in Polish). Górnictwo i Geologia, **5**: 31–39.

Bown, T.M., Kraus, M.J., 1981. Lower Eocene alluvial paleosols (Willwood Formation, Northwest Wyoming, U.S.A.) and their significance for paleoecology, paleoclimatology, and basin analysis. Palaeogeography, Palaeoclimatology, Palaeoecology, **34**: 1–30; https://doi.org/10.1016/0031-0182(81)90056-0

Bown, T.M., Kraus, M.J., 1987. Integration of channel and floodplain suites, I. Developmental sequence and lateral relations of alluvial paleosols. Journal of Sedimentary Petrology, **57**: 587–601; https://doi.org/10.1306/212F8BB1-2B24-11D7-8648000102C1865D

Card, C.J., Montenari, M., 2023. Comparative geochemistry of Early Carboniferous marine red beds (MRBs) and their significance for deep time paleoceanographic reconstructions. Sedimentary Geology, **444**: 106313; https://doi.org/10.1016/j.sedgeo.2022.106313

Choma-Moryl, K., 1988. Zmienność właściwości fizycznych iłów poznańskich okolic Wrocławia na tle ich genezy i litostratygrafii (in Polish). Geologia Sudetica, **23**: 1–63.

Christiansen, B.C., 2004. A transformational, structural and natural occurrence study of green rust. M.Sc. thesis, Äspö Hard Rock Laboratory, Geological Institute, University of Copenhagen, Denmark.

Ciuk, E., 1970. Lithostratigraphical schemes of the tertiary from the polish lowland area (in Polish with English summary). Kwartalnik Geologiczny, **14** (4): 754–771.

Ciuk, E., Pożaryska, K., 1982. On paleogeography of the Tertiary of the Polish Lowlands. Prace Muzeum Ziemi, **35**: 81–88.

Colombo, C. Palumbo, G., Di Iorio, E., Russo, F., Terribile, F., Jiang, Z., Liu, Q., 2016. Soil development in a Quaternary fluvio-lacustrine paleosol sequence in Southern Italy. Quaternary International, **418**: 195–207; https://doi.org/ 10.1016/j.quaint.2015.11.004

Cornell, R.M., Schwertmann, U., 2003. The Iron Oxides – Structure, Properties, Reactions, Occurrences and Uses, 2nd ed. Wiley-VCH Verlag, Weinheim; http://doi.org/10.1002/3527602097

Duczmal-Czernikiewicz, A., 2010. Geochemistry and mineralogy of the Poznań Formation (Polish Lowlands). Adam Mickiewicz University Press, Poznań.

Duczmal-Czernikiewicz, A., 2013. Evidence of soils and palaeosols in the Poznań Formation (Neogene, Polish Lowlands). Geological Quarterly, **57** (2): 189–204; https://doi.org/10.7306/gq.1082

Dyar, M.D., Agresti, D.G., Schaefer, M.W., Grant, Ch.A., Sklute, E.C., 2006. Mössbauer spectroscopy of earth and planetary materials. Annual Review of Earth and Planetary Sciences, **34**: 83–125; https://doi.org/ 10.1146/annurev.earth.34.031405.125049

Dyjor, S., 1970. The Poznań series in west Poland (in Polish with English Summary). Kwartalnik Geologiczny, **14** (4): 819–835.

Goldstein, J.I., Newbury, D.E., Michael, J.R., Ritchie, N.W., Scott, J.H.J., Joy, D.C., 2017. Scanning Electron Microscopy and X-ray Microanalysis. 4th edition. Springer, New York; https://doi.org/10.1007/978-1-4939-6676-9

Górniak, K., Szydłak, T., Sikora, W.S., Gaweł, A., Bahranowski, K., Ratajczak, T., 2001. Clay minerals in colourful rocks appearing over lignite deposits in Konin region (in Polish with English summary). Górnictwo Odkrywkowe, **43**: 129–139.

Górnicki, R., Błachowski, A., Ruebenbauer, K., 2007. Mössbauer Spectrometer MsAa-3. Nukleonika, **52** (suppl. 1): S7–S12.

Habashi, F., 2016. Pigments through the Ages. InterCeram, International Ceramic Review, **65**: 156–165; https://doi.org/10.1007/BF03401164

Hartemink, A.E., 2009. The depiction of soil profiles since the late 1700s. Catena, **79**: 113–127; https://doi.org/10.1016/j.catena.2009.06.002

Jiang, Z., Liu, Q., Roberts, A.P., Dekkers, M. J., Barrón, V., Torrent, J., Li, S., 2022. The magnetic and colour reflectance properties of hematite: From Earth to Mars. Reviews of Geophysics, **60**: e2020RG000698; https://doi.org/10.1029/2020RG000698

Johnson, C.A., 2014. Observations and Assessment of Iron Oxide Nanoparticles in Metal-Polluted Mine Drainage within a Steep Redox Gradient, and a Comparison to Synthetic Analogs. D.Ph. thesis, Virginia Polytechnic Institute and State University; https://doi.org/10.1071/EN13184

Kasiński, J.R., Słodkowska, B., 2016. Factors controlling Cenozoic anthracogenesis in the Polish Lowlands. Geological Quarterly, **60** (4): 959–974; https://doi.org/10.7306/gq.1321

Kędzior, A., Widera, M., Zieliński, T., 2021. Ancient and modern anastomosing rivers: insights from sedimentological and geomorphological case studies of the Triassic, Neogene and Holocene of Poland. Geological Quarterly, **65**: 54; http://doi.org/10.7306/gq.1623

Klęsk, J., 2023. Sulphur and its main minerals in the Poznań Clays (upper Neogene) – their influence on the sediment colour (in Polish with English summary). Przegląd Geologiczny, **71**: 249–254; http://doi.org/10.7306/2023.22

Klęsk, J., Błachowski, A., Diduszko, R., Kruszewski, Ł., Widera, M., 2022. Iron-bearing phases affecting the colour of upper Neogene clayey sediments from Dymaczewo Stare, west-central Poland. Geologos, **28**: 129–139; https://doi.org/10.2478/logos-2022-0010

Kraus, M.J., 1999. Paleosols in clastic sedimentary rocks: their geologic applications. Earth-Science Reviews, **47**: 41–70; https://doi.org/10.1016/S0012-8252(99)00026-4

Kraus, M.J., Aslan, A., 1993. Eocene hydromorphic paleosols: significant for interpreting ancient floodplain processes. Journal of Sedimentary Research, **63**: 453–463; https://doi.org/10.1306/d4267b22-2b26-11d7-8648000102c1865d

Kraus, M.J., Riggins, S., 2007. Transient drying during the Paleocene–Eocene Thermal Maximum (PETM): analysis of paleosols in the Bighorn Basin, Wyoming. Palaeogeography, Palaeoclimatology, Palaeoecology, **245**: 444–461; https://doi.org/10.1016/j.palaeo.2006.09.011

Kruszewski, Ł., 2013. Supergene sulphate minerals from the burning coal mining dumps in the Upper Silesian Coal Basin, South Poland. International Journal of Coal Geology, **105**: 91–109; https://doi.org/10.1016/j.coal.2012.12.007

Maciaszek, P., Chomiak, L., Wachocki, R., Widera, M., 2019. The interpretive significance of ripple-derived sedimentary structures within the late Neogene fluvial succession, central Poland. Geologos, **25**: 1–13; https://doi.org/10.2478/logos-2019-0001

Maciaszek, P., Chomiak, L., Urbański, P., Widera, M., 2020. New insights into the genesis of the "Poznań Clays" – upper Neogene of Poland. Civil and Environmental Engineering Reports, **30**: 18–32; https://doi.org/10.2478/ceer-2020-0002

Mancini, M., Weindorf, D.C., Carvalho Monteiro, M.E., Gomes de Faria, Á.J., dos Santos Teixeira, A.F., de Lima, W., Dias de Lima, F.R., Santos Branco Dijair, T., D'Auria Marques, F., Ribeiro, D., Godinho Silva, S.H., Chakraborty, S., Curi, N., 2020. From sensor data to Munsell colour system: Machine learning algorithm applied to tropical soil colour classification via Nix™ Pro sensor. Geoderma, **375**: 114471; https://doi.org/10.1016/j.geoderma.2020.114471

McBride, E.F., 1974. Significance of colour in red, green, purple, olive, brown, and grey beds of Difunta Group, northeastern Mexico. Journal of Sedimentary Petrology, **44**: 760–773; https://doi.org/10.1306/212F6B9A-2B24-11D7-8648000102C1865D

Mills, S.J., Christy, A.G., Génin, J.-M.R., Kameda, T., Colombo, F., 2012. Nomenclature of the hydrotalcite supergroup: natural layered double hydroxides. Mineralogical Magazine, **76**: 1289–1336; https://doi.org/10.1180/minmag.2012.076.5.10

Mindat, 2022. Hudson Institute of Mineralogy, 1993–2022; https://www.mindat.org, retrieved 27.10.2022

Misol, A., Jimenéz, A., Labajos, F.M., 2022. Use of Ethylamine, Diethylamine and Triethylamine in the Synthesis of Zn,Al Layered Double Hydroxides. Chemical Engineering, **6**: 53; https://doi.org/10.1016/j.clay.2020.105539

Moore, D.C., Reynolds, R.C., 1997. X-ray Diffraction and the Identification and Analysis of Clay Minerals. Oxford University Press, Oxford.

Munsell Rock Color Book, 2012. Munsell Rock Color Book with genuine Munsell* colour chips. Geological Society of America (GSA).

Murad, E., 2010. Mössbauer spectroscopy of clays, soils and their mineral constituents. Clay Minerals, **45**: 413–430; https://doi.org/10.1180/claymin.2010.045.4.413

Murad, E., Cashion, J., 2004. Mössbauer spectroscopy of environmental materials and their industrial utilization. Kluwer Academic Publishers, Norwell, Massachusetts; https://doi.org/10.1007/978-1-4419-9040-2

Muslim, R.Q., Ritung, S., 2021. Distribution of pyrite depth and soil properties in fresh water swampland in North Candi Laras Sub-district, South Kalimantan Province. IOP Conf. Series: Earth and Environmental Science, **648**: 012041; https://doi.org/10.1088/1755-1315/648/1/012041

Myrow, P.M., 1990. A new graph for understanding colors of mudrocks and shales. Journal of Geological Education, **38**: 16–20; https://doi.org/10.5408/0022-1368-38.1.16

Myrow, P.M., 2003. Colours of Sedimentary Rocks. In: Encyclopedia of Sediments and Sedimentary Rocks (ed. G.V. Middleton): 159–161. Kluwer Academic Publishers, Dordrecht.

Nemec, W., Porębski S., 1977. Weissliegendes sandstones: a transition from fluvial-aeolian to shallow-marine sedimentation (Permian of the Fore-Sudetic Monocline). 2. A study in significance of rock colouration. Annales Societatis Geologorum Poloniae, **47**: 513–544.

Neuhuber, S., Wagreich, M., Wendler, I., Spötl, C., 2007. Turonian oceanic red beds in the eastern Alps: Concepts for palaeoceanographic changes in the Mediterranean Tethys. Palaeogeography, Palaeoclimatology, Palaeoecology, **251**: 222–238; https://doi.org/10.1016/j.palaeo.2007.03.049

Nørlund Christensen, A., Jensen, T.B., Bahl, C., DiMasi, E., 2007. Nano size crystals of goethite, -FeOOH: Synthesis and thermal transformation. Journal of Solid State Chemistry, **180**: 1431–1435; https://doi.org/10.1016/j.jssc.2007.01.032

Petit, S., Baron, F., Decarreau, A., 2017. Synthesis of nontronite and other Fe-rich smectites: a critical review. Clay Minerals, **52**: 469–483; https://doi.org/10.1180/claymin.2017.052.4.05

PiPujol, M.D., Buurman, P., 1994. The distinction between ground-water gley and surface-water gley phenomena in Tertiary paleosols of the Ebro basin, NE Spain. Palaeogeography, Palaeoclimatology, Palaeoecology, **110**: 103–113; https://doi.org/10.1016/0031-0182(94)90112-0

Piwocki, M., Ziembińska-Tworzydło, M., 1997. Neogene of the Polish Lowlands – lithostratigraphy and pollen-spore zones. Geological Quarterly, **41** (1): 21–40.

Piwocki, M., Badura, J., Przybylski, B., 2004. Neogen (in Polish). In: Budowa geologiczna Polski (eds. T.M. Peryt and M. Piwocki). Stratygrafia, 3a. Państwowy Instytut Geologiczny, Warszawa.

Ratajczak, T., Hycnar, E., Bożęcki, P., 2015. Mineralogical criterion as a part of suitability assessment of some Polish clay deposits for construction of waterproofing apertures. Wydawnictwo Instytutu Gospodarki Surowcami Mineralnymi i Energią PAN, Kraków.

Retallack, G.J., 2019. Soils of the Past. An Introduction to Paleopedology. 2nd edition. Wiley-Blackwell, Chichester.

Retallack, G.J., Broz, A.P., 2020. Ediacaran and Cambrian paleosols from central Australia. Palaeogeography, Palaeoclimatology, Palaeoecology, **560**: 110047; https://doi.org/10.1016/j.palaeo.2020.110047

Rickard, D., Luther, G.W., 2005. Metal sulfide complexes and clusters. Reviews in Mineralogy & Geochemistry, **61**: 421–504; https://doi.org/10.2138/rmg.2006.61.8

Rickard, D., Luther, G.W., 2007. Chemistry of iron sulfides. Chemical Reviews, **107**: 514–562; https://doi.org/10.1021/cr0503658

Ruban, D.A., Mikhailenko, A.V., Yashalova, N.N., 2021. The power of colour in geoheritage studies and marketing: some tentative reflections. Geologos, **27**: 57–65; https://doi.org/10.2478/logos-2021-0005

Schwertmann, U., 1985. The effect of pedogenic environments on iron oxide minerals. Advances in Soil Science, **1**: 171–200; https://doi.org/10.1007/978-1-4612-5046-3_5

Schwertmann, U., 1993. Relations between iron oxides, soil colour, and soil formation. Soil Science Society of America, Special Publications, **31**: 51–69; https://doi.org/10.1007/BF03161698

Shepard, F.P., 1954. Nomenclature based on sand-silt-clay ratios. Journal of Sedimentary Research, **24**: 151–58.

Song, H., Jiang, G., Poulton, S.W., Wignall, P.B., Tong, J, Song, H., An, Z., Chu, D., Tian, L., She, Z., Wang, C., 2017. The onset of widespread marine red beds and the evolution of ferruginous oceans. Nature Communications, **8**: 399; https://doi.org/10.1038/s41467-017-00502-x

Spinola, D.N., de Castro Portes, R., Srivastava, P., Torrent, J., Barrón, V., Kühn, P., 2018. Diagenetic reddening of Early Eocene paleosols on King George Island, Antarctica Geoderma, **315**: 149–159; https://doi.org/10.1016/j.geoderma.2017.11.010

Srivastava, P., Patel, S., Singh, N., Jamir, T., Kumar, N., Aruche, M., Patel, R.C., 2013. Early Oligocene paleosols of the Dagshai Formation, India: A record of the oldest tropical weathering in the Himalayan foreland. Sedimentary Geology, **294**: 142–156; https://doi.org/10.1016/j.sedgeo.2013.05.011

Srivastava, S., Snellings, R., Meynen, V., Cool, P., 2021. Siderite-calcite ($FeCO_3$-$CaCO_3$) series cement formation by accelerated carbonation of CO_2(g)-H_2O-Fe-Ca$(OH)_2$ systems. Cement and Concrete Composites, **122**: 104137; https://doi.org/10.1016/j.cemconcomp.2021.104137

Stevens, J.G., Khansanov, A.M., Miller, J.W., Pollak, H., Li, Z., 2005. Mössbauer Mineral Handbook. Mössbauer Effect Data Center, 3rd edition. The University of North Carolina: Asheville, NC, USA.

Stucki, J.W., 2011. A review of the effects of iron redox cycles on smectite properties. Comptes Rendus Geoscience, **343**: 199–209; https://doi.org/10.1016/j.crte.2010.10.008

Środoń, J., 1999. Nature of mixed-layer clays and mechanisms of their formation and alteration. Annual Review of Earth and Planetary Sciences, **27**: 19–53; https://doi.org/10.1146/annurev.earth.27.1.19

Środoń, J., Drits, V.A., McCarty, D.K., Hsieh, J.C.C., Eberl, D.D., 2001. Quantitative XRD analysis of clay-rich rocks from random preparations. Clays and Clay Minerals, **49**: 514–528; https://doi.org/10.1346/CCMN.2001.0490604

Środoń, J., Szulc, J., Anczkiewicz, A., Jewuła, K., Banaś, M., Marynowski, L., 2014. Weathering, sedimentary, and diagenetic controls of mineral and geochemical characteristics of the vertebrate-bearing. Silesian Keuper. Clay Minerals, **49**: 569–594; https://doi.org/10.1180/claymin.2014.049.4.07

TCMS, 2022. The Clay Minerals Society, Reynolds Cup Competition, https://www.clays.org/reynolds, retrieved 27.10.2022.

Torrent, J., Schwertmann, U., Schulze, D.G., 1980. Iron oxide mineralogy of some soils of two river terrace sequences in Spain. Geoderma, **23**: 191–208; https://doi.org/10.1016/0016-7061(80)90002-6

Troć, M., Sadowska, A., 2006. The age of Poznań Formation in the area of Poznań (in Polish with English summary). Przegląd Geologiczny, **54**: 588–593.

Tucker, M.E., 2011. Sedimentary Rocks in the Field: A Practical Guide. Wiley-Blackwell, Chichester, UK; https://doi.org/10.1002/gj.1341

Turner, P., 1980. Continental Red Beds. Developments in Sedimentology, **29**. Elsevier, Amsterdam; https://doi.org/10.1346/CCMN.1981.0290115

Upreti, N., Srivastava, P., 2019. Role of latitudinal shift and climate change in evolution of red and yellow palaeosols of the Himalayas: Implications for early Oligocene seasonality and Mid-Miocene enhanced precipitation. Sedimentology, **67**: 2189–2221; https://doi.org/10.1111/sed.12699

Valanciene, V., Siauciunas, R., Baltusnikaite, J., 2010. The influence of mineralogical composition on the colour of clay body. Journal of the European Ceramic Society, **30**: 1609–1617; https://doi.org/10.1016/j.jeurceramsoc.2010.01.017

Wiewióra, A., Wyrwicki, R., 1974. Clay minerals in the mottled clay horizon of the Poznań series (in Polish with English summary). Kwartalnik Geologiczny, **18** (3): 615–635.

Wiewióra, A., Wyrwicki, R., 1976. Beidellite from the sediments of the Poznań series (in Polish with English summary). Kwartalnik Geologiczny, **20** (2): 331–341.

Widera, M., 2007. Lithostratigraphy and palaeotectonics of the sub-Pleistocene Cenozoic of Wielkopolska (in Polish with English summary). Wydawnictwo Naukowe UAM, Poznań.

Widera, M., 2021. Geologia polskich złóż węgla brunatnego (in Polish). Bogucki Wydawnictwo Naukowe, Poznań.

Widera, M., Kowalska, E., Fortuna, M., 2017. A Miocene anastomosing river system in the area of Konin Lignite Mine, central Poland. Annales Societatis Geologorum Poloniae, **87**: 157–168; https://doi.org/10.14241/asgp.2017.012

Widera, M., Chomiak, L., Zieliński, T., 2019. Sedimentary facies, processes and paleochannel pattern of an anastomosing river system: an example from the Upper Neogene of Central Poland. Journal of Sedimentary Research, **89**: 487–507; https://doi.org/10.2110/jsr.2019.28

Widera, M., Bechtel, A., Chomiak, L., Maciaszek, P., Słodkowska, B., Wachocki, R., Worobiec, E., Worobiec, G., Zieliński, T., 2021a. Palaeoenvironmental reconstruction of the Konin Basin (central Poland) during lignite accumulation linked to the Mid-Miocene Climate Optimum. Palaeogeography, Palaeoclimatology, Palaeoecology, **568**: 110307; https://doi.org/10.1016/j.palaeo.2021.110307

Widera, M., Zieliński, T., Chomiak, L., Maciaszek, P., Wachocki, R., Bechtel, A., Słodkowska, B., Worobiec, E., Worobiec, G., 2021b. Tectonic-climatic interactions during changes of depositional environments in the Carpathian foreland: An example from the Neogene of central Poland. Acta Geologica Polonica, **71**: 519–542; https://doi.org/10.24425/agp.2020.134567

Widera, M., Chomiak, L., Wachocki, R., 2023. Distinct types of crevasse splays formed in the area of Middle Miocene mires, central Poland: Insights from geological mapping and facies analysis. Sedimentary Geology, **443**: 106300; https://doi.org/10.1016/j.sedgeo.2022.106300

Wyrwicki, R., 1975. Mineral composition and economic value of variegated Poznań clays (Pliocene) (in Polish with English summary). Kwartalnik Geologiczny, **19** (3): 633–648.

Zachos, J., Pagani, M., Sloan, L., Thomas, E., Billups, K., 2001. Trends, rhythms, and aberrations in global climate 65 Ma to present. Science, **292**: 686–693; https://doi.org/10.1126/science.1059412

Zhitova, E.S., Krivovichev, S.V., Pekov, I.V., Yakovenchuk, V.N., Pakhomovsky, Ya.A., 2016. Correlation between the d-value and the M^{2+}:M^{3+} cation ratio in Mg-Al-CO_3 layered double hydroxides. Applied Clay Science, **130**: 2–11; https://doi.org/10.1016/j.clay.2016.01.031

Zieliński, T., Widera, M., 2020. Anastomosing-to-meandering transitional river in sedimentary record: A case study from the Neogene of central Poland. Sedimentary Geology, **404**: 105677; https://doi.org/10.1016/j.sedgeo.2020.105677

APPENDIX

Examples of varicoloured "Poznań Clays" exposed in opencast mines managed by the Konin Lignite Mine

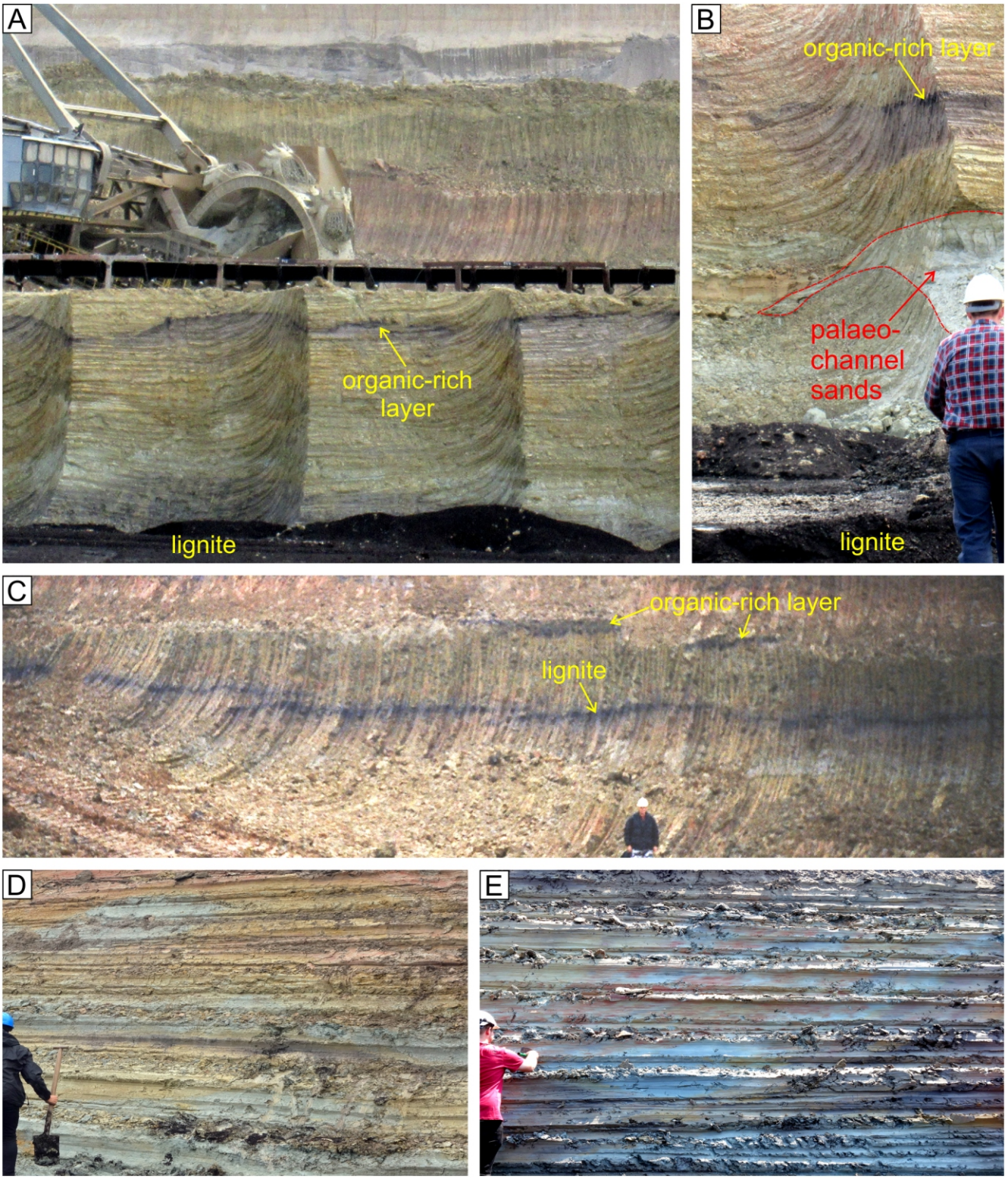

A–**C** – note, the presence of organic-rich and lignite layers (hydromorphic palaeosol horizons), and palaeochannel sands; **D**, **E** – close-up view of the sediments studied with colours ranging from bluish to red